Effect of viscosity on *Leishmania mexicana* motility

Rose Caroline Atieno Kitoyi

Master of Science by research

University of York

Biology

December 2023

ABSTRACT

Motility is important for the *Leishmania* parasite to survive, transition into the next host and differentiate into the mammalian infective form. There are several external factors that this parasite faces in its environment that could affect its movement. This research examined the impact of changes in viscosity on motility of *L. mexicana*, the causative organism for cutaneous leishmaniasis. Velocity, curvature, and helicity were used to describe observed motility. Known molecular markers were used to validate procyclic and metacyclic promastigote life cycle stages. Individual cell movement was tracked in 3D with digital inline holographic microscopy. Finally, polymer and fPPG samples that I carefully prepared were used to measure their viscosity using magnetic tweezers by L.G. Wilson.

In support of previous findings by Findlay *et al* (eLife, 2021), this study found that the human infective metacyclic promastigote cells swim faster in a 'run and tumble' behaviour, whereas the procyclic promastigote cells swim slower in a helical meandering pattern. Metacyclic promastigote cells display a lower swimming curvature compared to procyclic promastigote cells at comparable viscosities. Helicity was found to have an equitable, symmetrical distribution in both procyclic and metacyclic promastigote cells, without evident bias towards right or left handedness. Overall, these trends were repeated across different polymer and fPPG concentrations. The absolute viscosity measurements in Ficoll, PVP, and fPPG were comparable, showing an increase with rise in concentration.

The investigation of *L. mexicana* cell movement in fPPG, a biologically relevant environment, identified swimming mechanisms critical for the parasite to navigate and adapt to environmental constraints. Such pre-adaptation allows these parasites to alter their motility and maximise infection potential, promoting life cycle progression.

TABLE OF CONTENTS

DECLARATION

I declare that this thesis is a presentation of original work, and I am the sole author except where noted. This work has not previously been presented for a degree or other qualification at this University or elsewhere. All sources are acknowledged as references.

DEDICATION

To that person who must rise above the challenges that life throws at them and keep winning, anyway.

ACKNOWLEDGEMENTS

I am grateful for the support extended to me by numerous individuals during this research. While it is impossible to name everyone, I would like to convey my sincere gratitude to each of you.

A huge thank you to the York Graduate Research School (YGRS) for providing me with a studentship. Indeed, this opportunity has awoken a long-time dream of mine to work with parasites of medical importance. Thank you for believing in me. Special mention to the dean, Professor Kate Arnold for believing in my passion.

A massive thank you to my supervisors Dr. Pegine Walrad and Dr. Laurence Wilson. You both went above and beyond in supporting me and encouraging me throughout the project. Thank you for your taking the time to ensure that I grasped the technical components. When the story of my career will be written in the future, you will have a special place in it. I'd also like to acknowledge the members of the Walrad and Wilson Labs for their wonderful support throughout this project.

On a more intimate level, I'd like to express my gratitude to my family., especially my uncle Isaac Otieno. You have been there as a father figure ever since daddy passed on. You have provided a shoulder to lean on particularly when life threw some major curve balls my way. Thank you for calling me every single week from Kenya and checking on my mental health. I say a big thank you to my brother George Kitoyi and my sister Beatrice Kitoyi. Blood may have made us relatives, but love has made us friends. I treasure you both.

LIST OF FIGURES

LIST OF TABLES

LIST OF ABBREVIATIONS

2D	Two dimensional
3D	Three dimensional
µg	Micrograms
µL	Microlitres
µm	Micrometres
cDNA	Copy Deoxyribonucleic Acid
C1	Confidence Interval
CL	Cutaneous Leishmaniasis
CRISPR	Clustered Regularly Interspaced Short Palindromic Repeats
DALY	Disability Adjusted Life Years
DAT	Direct Agglutination Test
DIHM	Digital Inline Holographic Microscopy
dNTPs	Deoxynucleotide triphosphate
ds DNA	Double stranded deoxyribonucleic acid
DNA	Deoxyribonucleic Acid
dT	Deoxythymidine
ELISA	Enzyme-Linked Immunosorbent Assay
fPPG	Filamentous phosphoglycan
GPI	Glycosylphosphatidylinositol
GPILS	Glycosylinositolphospholipids
H&E	Hematoxylin and Eosin
HIV	Human Immunodefficiency Virus
ICT	Immunichromatograpy
Kb	Kilobases
kDa	Kilo Dalton
kDNA	Kinetoplast Deoxyribonucleic Acid
LED	Light Emitting Diode

LPG	Lipophosphoglycan
MCL	Mucocutaneouos Leishmaniasis
META	Metacyclic promastigotes
mRNA	messenger RNA
MT	Magnetic Tweezers
Ng	Nanograms
Nmt	N-myristoyltransferase
PBS	Phosphate buffered saline
PCF	Procyclic promastigotes
PCR	Polymerase Chain Reaction
PFR	Paraflagellor rod
PG	Phosphoglycan
PKDL	Post Kalar Azar Dermal Cutaneous Leishmaniasis
PM	Peritrophic Matrix
Poly A	Polyadenylated
PPG	Proteophosphoglycans
PSG	Promastogote Secretory Gel
PVP	Polyvinylpyrrolidone
qPCR	Quantitative polymerase chain reaction
RT-PCR	Reverse transcription polymerase chain reaction
rRNA	Ribosomal RNA
RNA	Ribonucleic Acid
RT	Reverse Transcriptase
RT-qPCR	Real-time quantitative reverse transcription polymerase chain reaction
sAP	Filamentous acid phosphatase
SHERP	Small hydrophilic endoplasmic reticulum associated protein
ssDNA	Single stranded deoxyribonucleic acid
SEM	Scanning Electron Micrograph
tRNA	transfer RNA

UTR	Untranslated region
UV	Ultra violet
VL	Visceral Leishmaniasis
WHO	World Health Organisation

1. GENERAL OVERVIEW AND REVIEW OF LITERATURE

1.1 General introduction

Leishmaniasis is a parasitic disease that disproportionately impacts the most economically disadvantaged individuals worldwide (1). It is prevalent in 98 countries spanning 5 continents, with 700,000 to 1 million new cases reported annually (2) resulting in approximately 50,000 fatalities (3). The risk of infection extends to 350 million individuals worldwide (4). According to published burden assessments, leishmaniasis ranks second in terms of mortality, trailing only behind malaria, and is the 4th most significant contributor to morbidity among parasitic diseases. Furthermore, the disease is associated with the loss of over 3 million disability-adjusted life years (DALYs) (5).

The disease is caused by a protozoan parasite from the genus *Leishmania*, specifically belonging to the subgenus *Leishmania* and *Viannia. The* primary mode of transmission is through sand flies, although instances of non-vector transmission, such as accidental laboratory infections, blood transfusions, or organ transplantations, are possible but infrequent (6).

Over the last two decades, there has been a notable increase in confirmed cases of cutaneous leishmaniasis on a global scale (7). Several factors have been identified as contributors to this surge, including globalisation, migration, conflicts, the prevalence of HIV (Human Immunodeficiency Virus), and climate change, among other factors (8). The correlation between conflict and visceral leishmaniasis has been consistently demonstrated (9). For instance, during the civil unrest in Ethiopia from 2002 to 2022, a significant number of affected individuals fled to other regions of the country that were known hotspots for visceral leishmaniasis (9). The crowded conditions in refugee camps, coupled with their remote locations, posed challenges for aid workers in delivering services, resulting in a notable rise in disease incidence (9).

Presently, South Sudan is grappling with civil unrest, raising concerns of a recurrence of the scenario observed in Ethiopia (9).

1.1.1 Clinical features

The virulence, pathogenicity, and clinical manifestations of the disease vary among species, with symptoms ranging from a self-healing cutaneous lesion at the insect bite site to a systemic abnormality in visceral organs that poses a severe threat to life (10).

1.1.1.1 Cutaneous leishmaniasis (CL)

Cutaneous leishmaniasis (CL) is the most prevalent form of the disease, affecting 0.7 to 1.3 million individuals worldwide annually (11). The disease results in skin lesions of diverse severity, which, while not life-threatening, may take 2 to 10 months to heal spontaneously, influenced by the severity of the lesions and the occurrence of secondary infections. The scars that remain after healing can contribute to self and social stigma (12). This form of leishmaniasis is caused by various species, including *Leishmania amazonensis, L. mexicana, L. braziliensis, L. panamesis, L. peruviana,* and *L. guayanensis* (In the Americas) (Figure 1.1a). Additionally, it is attributed to *L. infantum* (found in the Mediterranean and Caspian Sea regions), and *L. major, L. tropica, L. aethiopica* (In Europe, Asia and Africa) (Figure 1.2a) (13,14). The disease is further classified into anthroponotic CL, zoonotic CL, and diffuse CL, contributing to the complexity of diagnosis for CL (15).

1.1.1.2 Mucocutaneous leishmaniasis (MCL)

Approximately 1% to 10% of CL patients will progress to develop mucocutaneous leishmaniasis (MCL), characterised by severe and debilitating lesions affecting the mucosal membranes (16). The initial lesion forms on the skin due to *Leishmania* infection but eventually extends to the mucocutaneous region, involving areas such as the face, throat, larynx, and buccal cavity. These lesions are disfiguring and highly severe. The primary vector for MCL is *L. braziliensis* (17,18), although rare instances have been associated with *L. panamensis* and *L. guyanensis (*the Americas), occasionally *L. infantum, L. donovani* and *L. aethiopica* (Africa and Asia) (18).

1.1.1.3 Visceral leishmaniasis (VL)

Visceral leishmaniasis (VL) represents the most severe form of the disease, and without treatment, it proves fatal in over 95% of cases, with an estimated 0.2 to 0.4 million new cases reported annually worldwide. The figures have reduced in India (19). Symptoms of VL include weight loss, fever, hepatomegaly, splenomegaly (sometimes hepatosplenomegaly), and anaemia. These symptoms result from damage to the reticuloendothelial system cells, leading to enlargement (20). Given that fever and hyperpigmentation are two prominent symptoms of VL, the disease is commonly referred to as Kala Azar or "black fever" in Hindi (21). The term "dumdum" is also used for the disease. Risk factors include younger age, immunosuppression (such as HIV infection), and malnutrition. The causative agents of the disease are from the *L. donovani* complex, which comprises three species: *L. donovani, L. infantum*, and *L. chagasi*, although the composition of the complex has been debated (4). The prevalence of VL in Europe, Asia, Africa, and the Americas closely mirrors that of cutaneous leishmaniasis, although CL is found at much higher altitudes (Figures 1.1b & 1.2b).

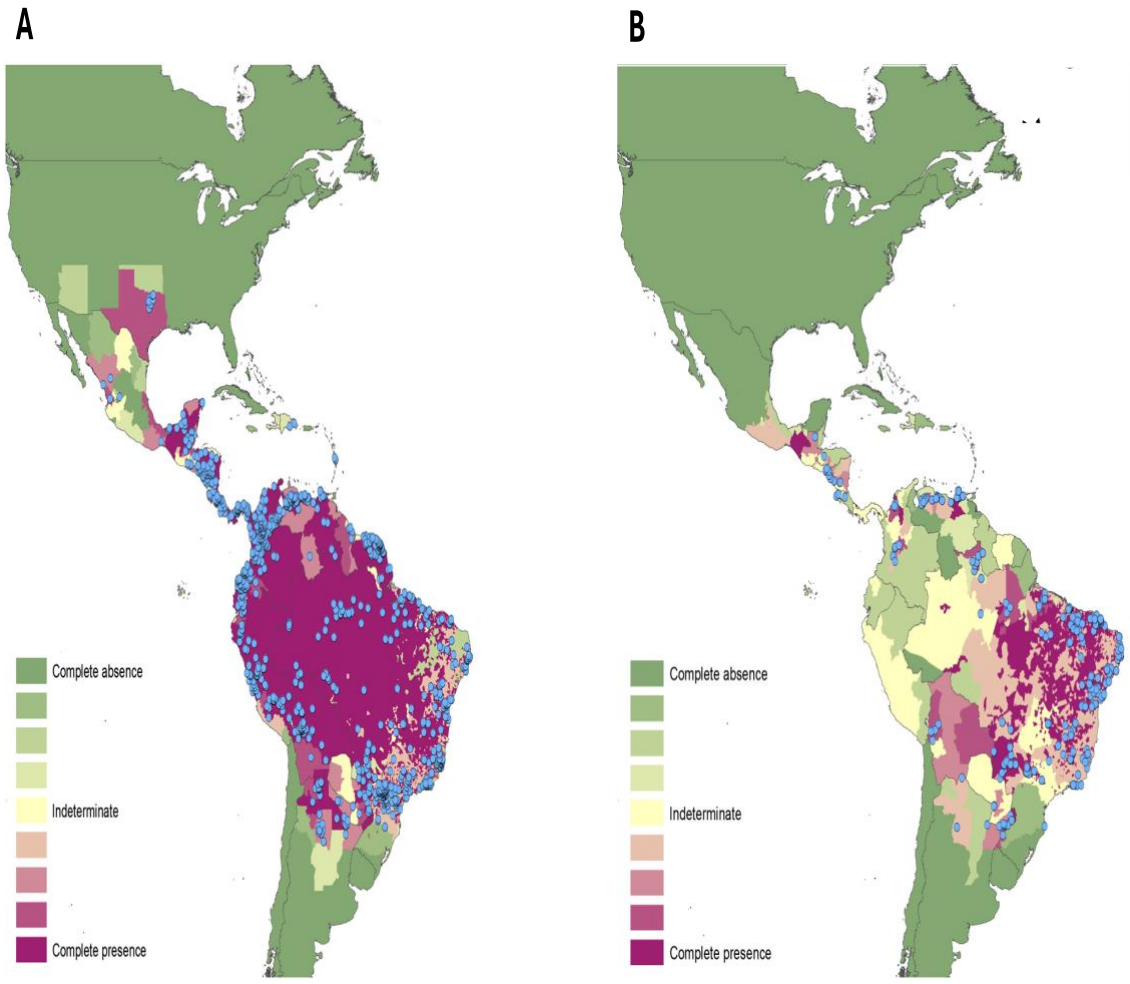

Figure 1.1: Documented spread of cutaneous (A) and visceral (B) leishmaniasis in the Americas. Evidence consensus for presence of the disease ranging from green (full agreement on the absence: −100%) to purple (total agreement on the presence). Adapted from (22)

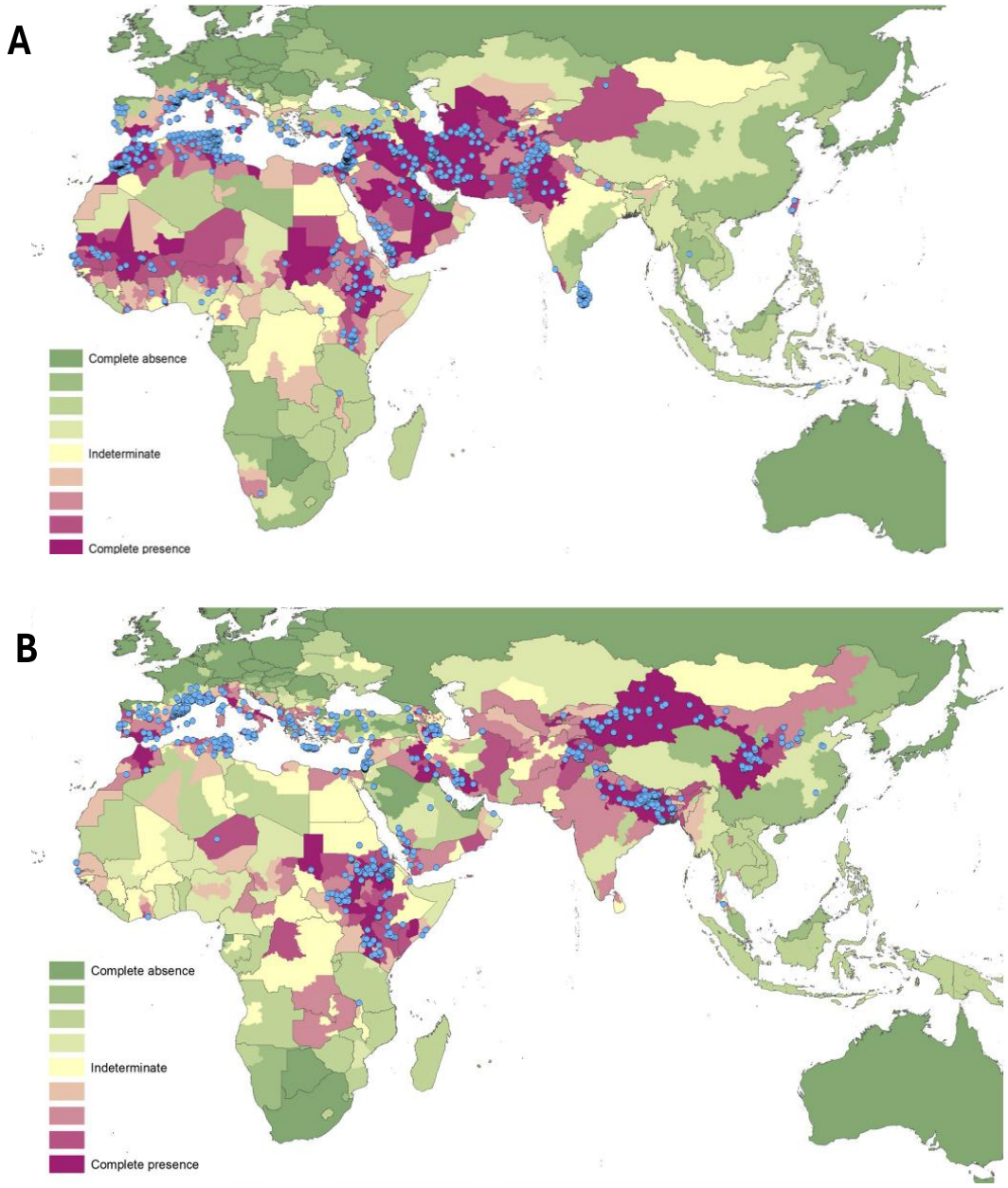

Figure1.2: Documented spread of cutaneous (A) and visceral (B) leishmaniasis in the Europe, Africa and Asia. Evidence consensus for presence of the disease ranging from green (full agreement on the absence: −100%) to purple (total agreement on the presence). Adapted from (22)

1.1.1.4 Post Kalar Azar Dermal Leishmaniasis (PKDL)

Post Kala Azar Dermal Leishmaniasis (PKDL) is a complication that can arise after recovering from VL. It is characterised by skin lesions, including papules, nodules, and patches, in a patient who has otherwise recovered from VL and is in good health. The rash typically initiates around the mouth and then gradually spreads to other parts of the body, the extent depending on severity. This is believed to be an evolutionary adaptation by the parasite, making it more likely to be picked up by sand fly thus increase chance of transmission. PKDL can manifest months to years after successful treatment and is confined to areas where *L. donovani* is the causative parasite (23).

Figure 1.3 provides an illustration of the various clinical manifestations of the disease discussed in sections 1.1.1.1 to 1.1.1.4 above.

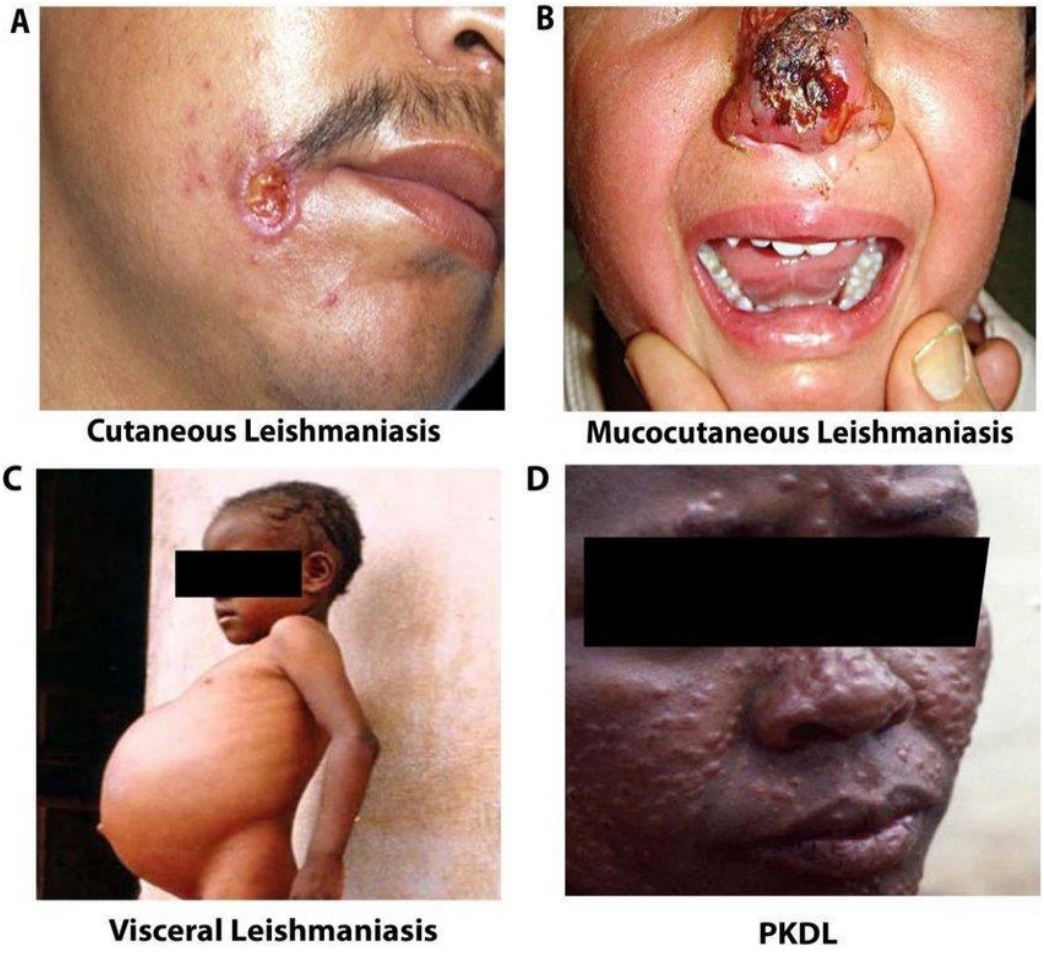

Figure1.3: Clinical signs of leishmaniasis. (A) Cutaneous leishmaniasis. (B) Mucocutaneous leishmaniasis. (C) Visceral leishmaniasis. (D) Post kala-azar dermal cutaneous leishmaniasis (PKDL) (24)

1.1.2 Diagnosis, treatment and control

1.1.2.1 Diagnosis

In addition to clinical manifestations, various parasitological and immunological tests are employed for the diagnosis of leishmaniasis. These include the direct microscopic examination of Giemsa-stained scrapings, impression smears and skin biopsies, applicable to mucocutaneous and cutaneous leishmaniasis (25). For VL, aspirates from spleen, liver, lymph nodes and bone marrow are examined using the same method (25). Microscopy is considered the gold standard for diagnosis, with Hematoxylin and Eosin (H&E) staining of tissue sections during histopathology aiding in parasite detection, particularly in cases with very low parasite doses (26,27). The primary diagnostic technique widely used in hospitals and research institutes is polymerase chain reaction (PCR) due to its high sensitivity. This method involves amplifying conserved sequences from the *Leishmania* kinetoplast or rRNA (ribosomal ribonucleic acid) gene (25,28). Immunological methods for leishmaniasis diagnosis encompass the Montenegro or Leishmanin skin test (based on delayed type hypersensitivity), antigen detection in urine using latex agglutination, serodiagnosis through indirect immunofluorescence, and ELISA (Enzyme-linked immunosorbent assay) (29). Furthermore, rapid immunological techniques such as rK39 ICT (Immunochromatography) (30) and DAT (Direct Agglutination Test) are employed for the diagnosis of the disease (31).

1.1.2.2 Treatment

Several medications are currently in use for the treatment of leishmaniasis, encompassing topical, oral, and parenteral formulations. Pentavalent antimonials, including meglumine antimonate and sodium stibogluconate, have been the primary drugs for over fifty years and remain the first-line treatment for CL in many regions (32). However, they are associated with significant limitations, including severe side effects and the emergence of drug resistance (33,34). The first line treatment for VL is ambisome (liposomal amphotericin B) in India (32).

Additionally, other medications available for leishmaniasis treatment include miltefosine, paromycin, and sitamaquine. Miltefosine is the only oral drug but is teratogenic (35).

In a general sense, the challenging aspects of treating the disease, particularly VL include the prolonged duration of treatment, the discomfort associated with injections (for toxic drugs), and extended hospital stays, which can last up to 2 months (9).

1.1.2.3 Prevention and control

There is currently no widely available effective human vaccine for leishmaniasis prevention (36). Typically, vaccines function by triggering an antibody response to a specific part of a pathogen and storing this memory on B cells, which subsequently produce antibodies. When the person is exposed to the pathogen again, these antibodies work to eliminate it (9). This approach has proven effective for bacteria and various viruses. In contrast, tackling malaria and *Leishmania* parasites has posed a challenge because they have developed mechanisms to hide within other cells, evading detection by antibodies. It is proposed that a T cell response is crucial in addressing this issue. T cells have the ability to recognise and eliminate infected cells. Nevertheless, eliciting a T cell response in humans is complex. Furthermore, studying and quantifying T cells is considerably more challenging than antibodies (9). In recent times, researchers have been exploring two distinct vaccine approaches for leishmaniasis. One method involves utilising engineered viruses known as adenoviral vectors to train the body's T cells, enabling them to identify and eliminate infected immune cells (9). This approach has demonstrated safety in studies (37). The other strategy involves the use of a live vaccine that is attenuated. This concept is inspired by the practices of the Bedouin people in the Middle East, who applied sores from infected individuals onto hidden areas of their children's skin—a practice known as leishmanisation. While this led to the development of skin lesions in children, once they recovered, they showed protection against future infections, suggesting that live parasites could confer immunity. However, this is not sterile immunity and reinfection could occur. Despite these efforts, the approval of a vaccine is estimated to be at least 5 to 7 years away (9).

Controlling leishmaniasis is difficult due the fact that the sand fly vectors do not require a water body to lay eggs, are silent and small in size (9). This, combined with other constraints such as insufficient funding for control programmes, makes it difficult to develop an effective control strategy. Furthermore, the variability in vector distribution and diversity of parasite species further compound the problem (38). Disease surveillance, prompt diagnosis and treatment of cases, integrated vector management, control of reservoirs, and public awareness campaigns are just a few of the measures that are currently in use to control leishmaniasis (39). There was a VL control programme in Bihar, India, which ran from 1958 to 1970. During these years, no cases of VL were documented in Bihar, but the disease returned shortly after the programme ended. (40). Recently, VL was eliminated from Bangladesh (41). Unfortunately, there is little in place to control CL.

1.1.3 The parasite

The genus *Leishmania* belongs to a group of protozoans that belong to the Trypanosomatidae family, falling under the order Kinetoplastida (42). Similar to many other protozoan parasites, *Leishmania* have a digenetic life cycle involving an insect vector and vertebrate host (Figure 1.4).

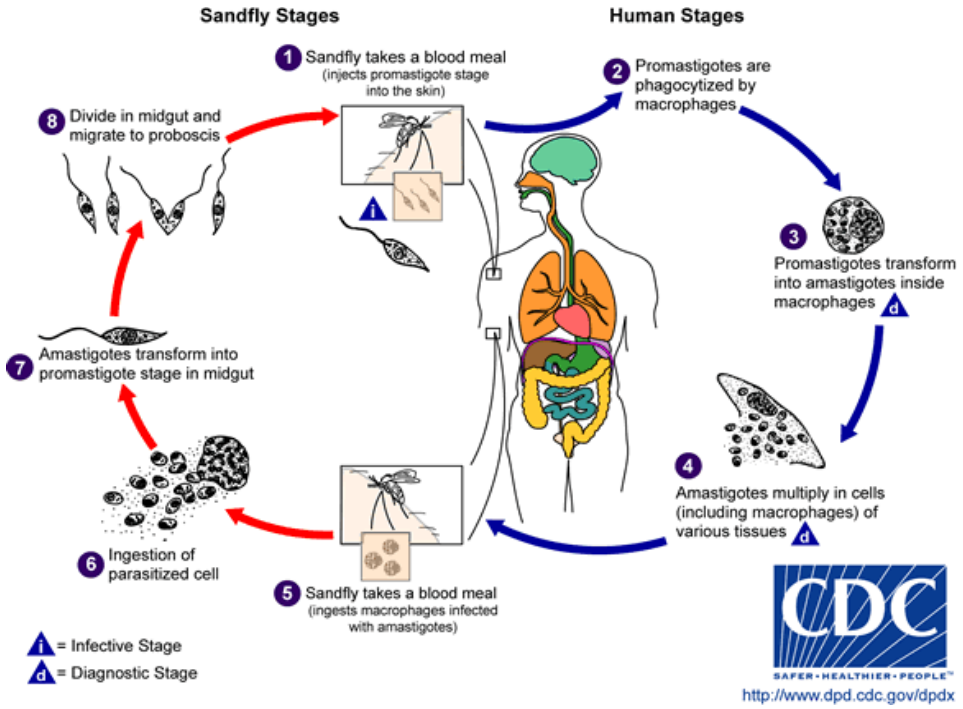

Figure 1.4: The life cycle of Leishmania in insect vector and vertebrate host Adapted from (43)

The parasite displays multiple cell morphologies and types adapted to either the vector or the mammalian host: intracellular amastigotes which reside and multiply within the phagolysosomal vacuole of host macrophage cells in mammals, and the 6 lifecycle stages of extracellular promastigotes sand fly vectors (44,45).

The multiple transformations that *Leishmania* undergoes in response to changes in its environment are remarkable. Each developmental form is specifically tailored to confront environmental challenges, providing it with a survival advantage. These adaptations encompass nutritional requirements, rate of development, capacity for division, expression of surface molecules, and morphology (46). Amastigotes, for example, are well adapted to survive within the intracellular parasitophorous vacuole in macrophages. They are non-motile since migration is unnecessary, and their small size (ranging from 3-5μm) allows them to thrive within a confined space. The length of their flagellum is significantly reduced, preventing its emergence from the flagellar pocket (47). Additionally, they are acidophiles, adapted to the acidic environment (48). Promastigotes exhibit distinct morphology compared to amastigotes. They possess a long, motile flagellum that extends out of the flagellar pocket and typically range in size from 15 to 30 μm in length (49). Remarkably, among all promastigote forms, metacyclic promastigotes, which are quiescent, are pre-adapted for mammalian survival and transmission to the next host. They express stage-specific surface molecules and are complement-resistant (46). In contrast, procyclic promastigotes are highly proliferative and complement-sensitive; eradicated by human serum (50). This illustrates that adaptation occurs not only for the current environment but also in anticipation of the next predicted shift in the environment.

So far, we have established that adaptation of protozoan parasites through their morphology is a mechanism for coping with environmental stress, granting a competitive edge for survival. The *Leishmania* parasite cell is composed of several organelles, including the flagellum, kinetoplast, and plasma membrane (44).

1.1.3.1 The flagellum

Motility is important for *Leishmania* parasite as it serves multiple roles, including parasite's attachment to the gut wall and migration. *Leishmania* flagellum structure is illustrated in Figure 1.5 below. Figures 1.5a and 1.5b illustrate the different external structures of the amastigote and promastigote flagellum, whereas Figures 1.5c, 1.5d and 1.5e depict their internal structures. The immobilisation of amastigote forms in the absence of an external flagellum (Figure 1.5a) emphasises the flagellum's crucial role in motility, making it the primary contributor to migration (51). This observation also highlights the variability within a single organism's ability to modify shape and, consequently, function for a particular lifecycle stage (52). On the other hand, the promastigote possesses a long, motile flagellum (Figure 1.5b) that extends out of the flagellar pocket. It is comprised of a filamentous paraflagellar rod (PFR) ((Figure 1.5c and 1.5d) that runs parallel to the standard 9+2 microtubular axoneme (44).

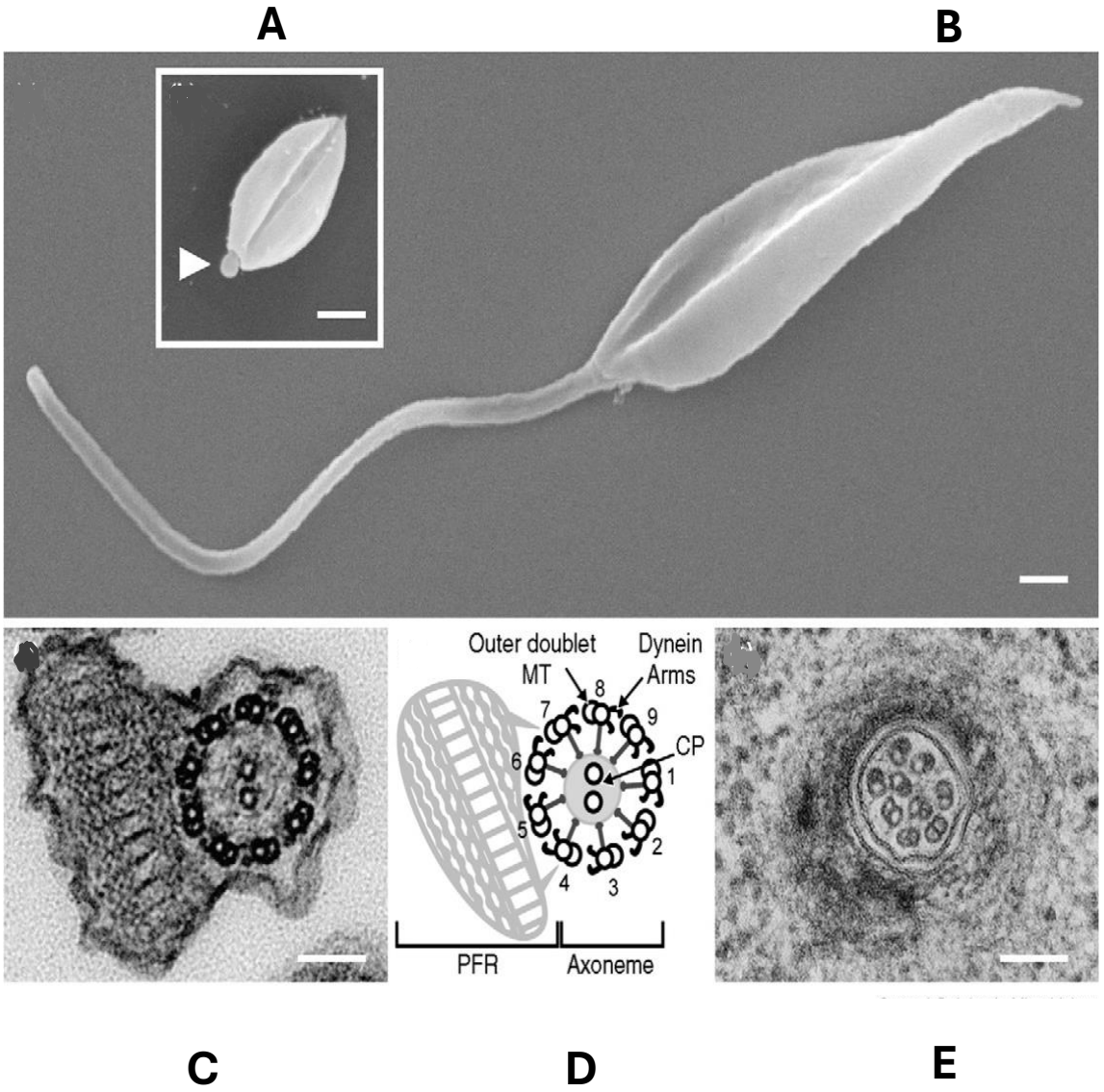

Figure 1.5: Leishmania flagellum structure in amastigote and promastigote. Scanning electron micrographs showing the difference in flagellum length between L. mexicana amastigote (A) and promastigote (B), with only the tip of the short amastigote flagellum exposed to the environment (arrowhead). Transmission electron micrographs of flagellum cross-sections showing promastigote and amastigote axoneme morphology (C and E). The promastigote PFR (shown in cartoon form in D). Adapted from (53)

The axoneme serves as a mechanical framework for all the enzymatic and mechanical components required to generate bending waves, with microtubules occurring in two forms: inner and outer arm dyneins. The outer arm dyneins act as amplifiers, increasing beat frequency and power output (54), and they are connected to inner arm dyneins, responsible for initiating and propagating flagellar bending (55). Dyneins play a key role in generating sliding between microtubular doublets, a motion that can be transformed into bending of the axoneme through local variations in dynein activation or sliding resistance along the length of the flagellum (54).

While the structural composition of the flagellum remains consistent across eukaryotes, they exhibit different types of movement, resulting in distinct swimming trajectories (55). Motility parameters in *Leishmania* can vary even within a single cell due to changes in the structure, length, and function of the flagellum (55). Presently, there is limited understanding of the control mechanisms operating within the flagella of *Leishmania* that produce local differences and generate diverse bending patterns.

The amastigote flagellum, as previously mentioned, is short and immobile, barely extending from the flagellar pocket. In amastigotes, the PFR is absent (41), resulting in an axoneme structure of 9+0 or 9V (Figure 1.5e). This flagellum is proposed to play a sensory role, as the 9V axonemal architecture is structurally similar to that found in mammalian primary cilia. Moreover, the tip of the flagellum in the *Leishmania* amastigote is often found in close contact with the parasitophorous vacuole membrane (44). Through its flagellum, the parasite might potentially sense the 'health' of its host macrophage by analysing crucial chemicals such as adenosine nucleotides. For instance, the parasite may decide to divide if the macrophage is deemed "healthy," but it may choose not to divide if the macrophage is considered "unhealthy" and is expected to undergo cell death and lysis, consequently releasing the parasite into a new environment (44). This implies the likely existence of checkpoints applied at different cell cycle stages (44). Additionally, researchers speculate that the parasite's release is unlikely to be a “passive” process but rather one driven by the parasite itself (44). The precise cell biology of the parasite's cell-cycle-related release, which remains an area of interest and importance, has not been thoroughly explored (44).

1.1.3.2 The kinetoplast

Leishmania spp is classified as a kinetoplastid due to possessing a kinetoplast in its mitochondrion. Other parasites that share this characteristic, containing kinetoplast DNA (kDNA), include *Trypanosoma brucei* and *T. cruzi*, responsible for severe human diseases like African sleeping sickness and Chagas disease respectively (56).

Kinetoplast DNA was initially described as 'a small spherical or rod-shaped structure lying just posterior to the basal body of the flagellum' (56).

The kDNA network is approximately 10 mm by 15 mm in size and consists of two DNA ring types: 5,000-10,000 minicircles and 25-50 maxicircles. Minicircles vary in size from 0.5 to 10 kilobases (kb) depending on the species, while maxicircles reach 20 to 40 kb. All DNA minicircles and maxicircles are linked in a massive DNA catenane, giving kDNA its distinctive chainmail structure (56).

Despite accounting for around 30% of parasite DNA, the functional significance of kDNA in *Leishmania* infections remains poorly understood. Interestingly, kDNA is found in the tissues of patients with Chagas disease and correlates with inflammatory cell infiltration. This evidence suggests that kDNA may play a role in immune recognition, modifying the immune response during an infection (57).

1.1.3.3 The plasma membrane

The plasma membrane in *Leishmania* is continuous and can be divided into three parts: the flagellar membrane, the flagellar pocket, and the pellicular plasma membrane (44).

The flagellar pocket, a deep invagination at the base of the flagellum, serves as the only site for exocytosis and endocytosis in the cell, making it a crucial interface between the parasite and its hosts. This pocket undergoes restructuring during differentiation (44). In amastigotes, the flagellar pocket is closed off at the neck, which is believed to be a protective measure for a potentially vulnerable area of the cell from the acidic and protease-filled environment within the parasitophorous vacuole. On the other hand, the promastigote flagellar pocket is open at the neck (44).

Indeed, comparing the morphology of the *Leishmania* amastigote flagellar pocket with that of the closely related organism *T. cruzi* would be intriguing. *T. cruzi*, as a related parasite, presents a unique scenario as it escapes from the parasitophorous vacuole and proliferates in a distinctly different environment—the cytoplasm of its host cell. Such a comparative analysis could provide valuable insights into the adaptations and strategies employed by these organisms in their interactions with host cells and their respective intracellular environments. On the other hand, the more open necked flagellar pocket in promastigotes may facilitate easier access to the flagellar pocket, allowing the parasite to intake large macromolecules and potentially influencing its motility (44).

The flagellar membrane, which envelops the flagellum, contains membrane proteins that play a role in sensing and signaling, such as LmjAQP1 (58) and ISO1 (58), among others.

The pellicular plasma membrane covers the entire cell surface and is adorned with densely packed microtubules and a glycolipid lipophosphoglycan (LPG) coat. This coat contains numerous permeases for nutrient uptake, such as LmGT2 and LmGT3 (51).

1.1.4 Morphometrics

The kinetoplast, along with morphological changes, serves as a valuable indicator for determining progression within the life cycle of *Leishmania* (56). A crucial parameter for this determination is the kinetoplast's position in relation to other cell organelles, specifically the nucleus and flagellar pocket. The relative positions of the nucleus, flagellar pocket, and kinetoplast vary along the anterior/posterior axis of the parasite's cell body. As the kDNA is consistently located posterior to the flagellar pocket but closely associated with the basal body, the morphological definition is based on the position of the kDNA relative to the nucleus. This classification results in 4 main morphological types of kinetoplasts, each defined by changes in the kDNA relative to the nucleus: trypomastigotes, epimastigotes, promastigotes, and amastigotes, as illustrated in Figure 1.6. Additionally, variations in *Leishmania* promastigote morphologies have been observed, and due to significant differences in their reported shapes (Figure 1.7), they are defined as different cell types or developmental forms rather than just transition morphologies (56).

These developmental forms are characterised based on criteria such as cell body length, cell body width, and flagellum length (59). Table 1.1 provides a summary of the morphological categorisation criteria for *L. mexicana.*

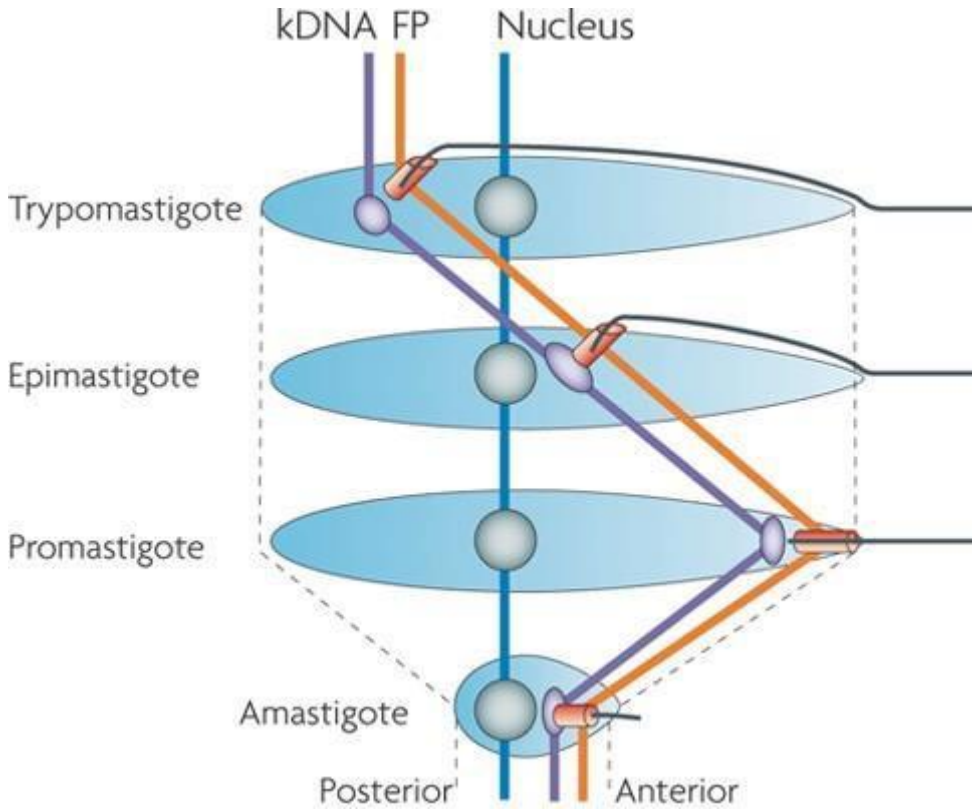

Figure 1.6: Kinetoplast location with regard to organelles during a flagellate's life cycle. FP flagellar pocket, kDNA, kinetoplast DNA. Adapted from (60)

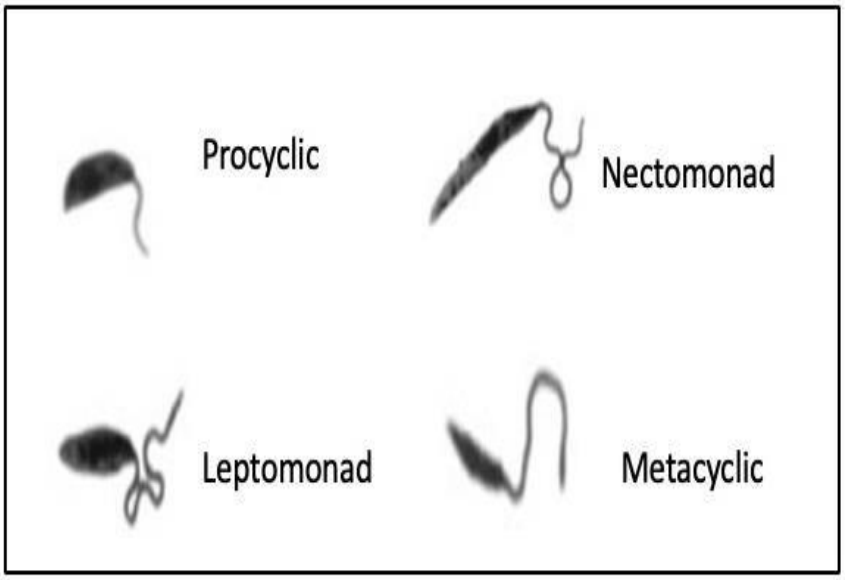

Figure1.7: The main promastigote morphologies in the sand fly during a Leishmania infection. Adapted from (44)

Morphological category	Criteria
Amastigote	Round body No visible flagellum
Procyclic	Body length 6.5-11.5µm Flagellum < Body length
Nectomonad	Body length ≥ 12µm
Leptomonad	Body length 6.5-11.5µm Flagellum ≥ Body length
Haptomomad	Expansion of flagellum tip
Metacyclic	Body length ≤ 8µm Body width≤ 1µm Flagellum >Body length
Paramastigotes	Kinetoplast adjacent to nucleus Visible flagellum present

Table 1.1: Morphological categorisation criteria for L. mexicana. Adapted from (59)

In summary, the cell morphology of *Leishmania* parasites is meticulously defined by factors such as cell shape, flagellum length, kinetoplast/nucleus position, and ultrastructural features. These characteristics have traditionally been instrumental in identifying and categorising various cell types. Importantly, certain morphological descriptions of cell shapes have become established in the literature as defining specific cell types within the life cycle. Crucially, there are currently limited molecular markers available to assist in more precise characterisations of life cycle forms (44). As a result, caution should be exercised when categorising cell types solely based on their shape, highlighting the need for further molecular insights to complement morphological classifications.

1.1.5 Sand fly vector

Sand flies are dipteran insects belonging to family Psychodidae (61). More than 800 species of sand flies have been identified. Only 98 of these more than 800 species have been confirmed or linked to the transmission of the human *Leishmania* parasite (62,63): 56 *Lutzomyia* species and 42 *Phlebotomus* species (62). Intriguingly, midges, dipteran insects belonging to the Ceratopogonidae family, have also been associated with the spread of leishmanial parasites in regions where phlebotomine sand flies are few or non-existent (64,65).

1.1.5.1 Sand fly feeding

Both female and male sand flies depend on obtaining a source of carbohydrates for energy, acquired through direct feeding on plant tissues and honeydew produced by aphids and coccids, referred to as the sugar meal phase (66). In the case of female sand flies, an additional protein source is essential to support egg development, known as the blood meal phase. The hematophagous nature of female sand flies, requiring a blood meal, facilitates the movement of the *Leishmania* parasite to and from the sand fly vector during feeding, making the sand fly an ideal carrier (67).

When acquiring both a blood meal and a sugar meal, the sand fly utilises its proboscis, but these meals follow distinct paths within the sand fly. The blood meal travels through the stomodeal valve and is enclosed by a sac-like structure called the peritrophic matrix (PM) in the midgut of the insect (68). In contrast, the sugar meal takes a different route down the stomodeal valve into the sand fly gut; it is swiftly redirected into the crop (69). This separation is crucial, as the sugar meal in the crop may contain substances that could impede the digestion of blood (70).

1.1.6 *Leishmania* development in the sand fly

Within the sand fly, *Leishmania* faces several bottlenecks and crucial tasks for a chance at transmission (67). These include multiplying, navigating to the sand fly's anterior midgut and mouthparts, and transforming into the only mammal-infective promastigote form, known as the metacyclic promastigotes (71). However, the journey is fraught with obstacles, and *Leishmania* must surmount several barriers to effectively colonise the sand fly. These challenges include:

(i) Overcoming the sand fly's digestive enzymes.

(ii) Evading the PM that encases the blood meal.

(iii) Resisting expulsion during the sand fly's defecation of the digested blood meal.

(iv) Travelling towards the proboscis counter to the digestive current.

(v) Withstanding the vector’s immune response, which involves lectins and antibacterial peptides (71).

In the subsequent discussion of the parasite's life cycle. I will elaborate on the mechanisms employed by *Leishmania* to overcome these challenges.

1.1.6.1 Life cycle

Pool-feeding sand flies utilise their mouthparts to incise their host's skin, causing the rupture of dermal capillaries and the formation of a blood pool (71). This method differs from that of mosquitoes, which exhibit more precise targeting during insertion to minimise damage to adjacent tissues and blood vessels.

During the biting process, sand flies release saliva into the wound, an essential component for blood-feeding due to its vasodilatory and antihaemostatic properties (72).

Parasites typically undergo exclusive midgut development within the sandfly, with the duration for complete growth ranging from 6 to 9 days on average, contingent on both species-specific factors and environmental conditions (72,73). The initial 48 hours are particularly crucial for transmission, as up to 50% to 80% of parasites may be lost during this period (59).

Amastigotes ingested in the posterior midgut undergo differentiation into poorly motile procyclic promastigotes within the PM during the initial 24 hours. The specific mechanisms governing this differentiation remain to be understood; however, temperature and pH are known cues (74).

The midgut epithelium actively secretes the PM in response to blood feeding, and its complete formation occurs within 6 to 24 hours post blood-meal, varying with the sand fly species. The PM serves a dual role: firstly, it provides physical protection to the midgut epithelium of the sand fly, shielding it from potential damage caused by pathogens present in the midgut lumen. Secondly, the PM, enclosing the blood meal containing *Leishmania* parasites offers protection to the parasites against the sand fly's digestive proteases. Since *Leishmania* parasites cannot traverse the PM before its disintegration, the PM provides an additional advantage for the procyclic promastigotes by keeping them confined, thus preventing their anterior movement and subsequent defecation (74).

The sand fly's digestive enzymes, including midgut proteases, and lectins reduce the survival ability of promastigotes, typically peaking in the first 18 to 48 hours. Notably, parasites seem to have the capability to suppress and delay the peak activity of midgut proteases (75). Additionally, they prevent parasite agglutination by sand fly lectins through a mechanism that remains unexplained (76).

During the procyclogenesis differentiation process from amastigote into the procyclic promastigote form, there is a ten-fold swelling and change in cell shape from the spherical amastigote to a more elongated ovoid shape as the flagellum extends (77).

Procyclic promastigotes undergo further differentiation into forms referred to as nectomonad promastigotes after 2 to 3 days. These nectomonad promastigotes escape the PM, attach to the midgut epithelium, and progress forward in the gut. They utilise lipophosphoglycan (LPG) on the surface of their flagellum to attach to glycoconjugates on the microvilli in the midgut (44). The natural movement of the midgut, propelling its contents towards the anus for excretion, necessitates the parasite's escape from the PM to avoid being expelled. Both the parasite and the sand fly release chitinases to facilitate the disintegration of the PM (74). Research indicates that the initiation of PM disintegration often occurs at the anterior and posterior ends (77). To further evade excretion, the parasite employs another mechanism by secreting a myoinhibitory peptide. This peptide reduces sand fly stomach peristalsis, thereby delaying defecation (20). This behavioural adaptation promotes the survival of the parasite in the midgut.

Nectomonad promastigotes, due to changes in LPG structure, will detach from the sand fly's midgut epithelium, migrate towards the thoracic midgut and stomodeal valve. In this new location, they undergo differentiation into leptomonad promastigotes. Leptomonad promastigotes, characterised by their highly replicative nature, multiply within the thoracic midgut over a span of 4 to 7 days. Notably, these parasites secrete a viscous, gel-like substance known as fPPG (filamentous phosphoglycan) (78).

Studies have demonstrated the existence of haptomonad promastigotes whose hemi-desmosome-like structures share similarities with those observed in attached epimastigote forms of trypanosomes, suggesting that attachment to the insect vector via such structures could be a common feature among all kinetoplastids. The biochemical composition of these structures is presently unknown, but uncovering the molecular components holds promise for significant revelations, given their importance in various kinetoplastid species (44). During sand fly feeding, the robust attachment of *Leishmania* haptomonad promastigotes to the stomodeal valve likely impedes their transmission to the mammalian host. This mechanism may play a crucial role in sustaining a long-term infection in the sand fly and/or facilitating asymmetric division (44).

Leptomonad promastigotes undergo further differentiation, eventually transforming into metacyclic promastigotes within the PSG. Metacyclic promastigotes exhibit slender bodies and flagella of approximately 20 μm in length, rendering them highly motile. Importantly, these metacyclic promastigotes represent the only promastigote stage that is infective to mammals. The metacyclic forms aggregate in the cardia region behind the stomodeal valve. Upon a sand fly bite, the regurgitation process involves the expulsion of PSG, sand fly saliva, and metacyclic promastigotes (59). In the absence of regurgitation, metacyclic stages can swim through the proboscis.

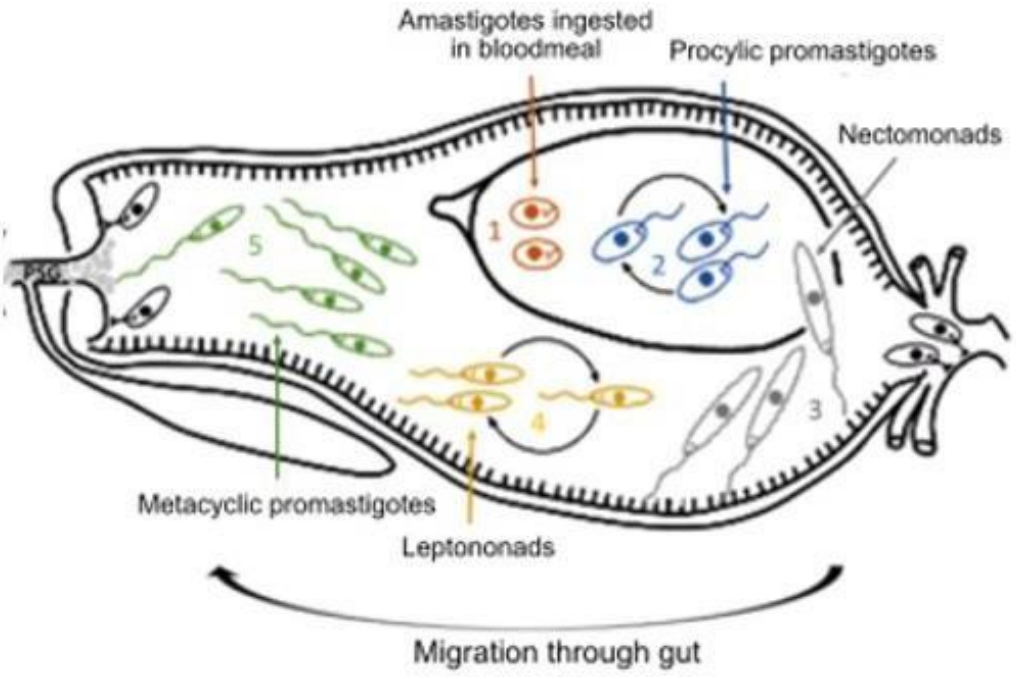

Figure 1.8: Leishmania parasite developing within the digestive tract of a competent vector, showcasing the time-dependent emergence of distinct morphological forms of promastigotes as they traverse the gut. Adapted from (79)

Our comprehension of the *Leishmania* parasite life cycle is continuously evolving, with recent research revealing the existence of an additional lifecycle stage known as retroleptomonad promastigotes (80,81). The differentiation of metacyclic promastigotes into retroleptomonad promastigotes occurs when *Leishmania*-infected sand flies take a second uncontaminated blood meal. Notably, retroleptomonad promastigotes exhibit a robust proliferative capacity and undergo rapid multiplication before eventually differentiating back into metacyclic promastigotes at a much faster and very different rate than leptomonad promastigotes. This process enhances the infectivity of sand flies, as it results in an increased number of infective metacyclic promastigotes (82).

1.1.7 *Leishmania* surface coat

Leishmania promastigotes are enveloped by a dense surface glycocalyx, predominantly comprised of molecules attached via glycosylphosphatidylinositol (GPI) anchors (82). These GPI-anchored molecules include proteins like the parasite surface protease gp63, proteophosphoglycans (PPGs), and short GPI-anchored glycosylinositolphospholipids (GIPLs). These surface molecules collectively form a protective surface coat and play a crucial role in mediating essential host-parasite interactions. Among these molecules, the most abundant is a large GPI-anchored phosphoglycan known as lipophosphoglycan (LPG) (83).

In all *Leishmania* species, the GPI anchor of LPG consists of a 1-O-alkyl-2-lysophosphatidylinositol lipid anchor and a heptasaccharide core. This core is connected to a long phosphoglycan (PG) polymer comprising 15 to 30 repeating units of [Galβ1,4Manα1-PO4] (substituted with other sugars in some species). The PG polymer is terminated by a capping oligosaccharide (84). Figure 1.9 is a schematic representation of *Leishmania* LPG structure, highlighting 4 key domains.

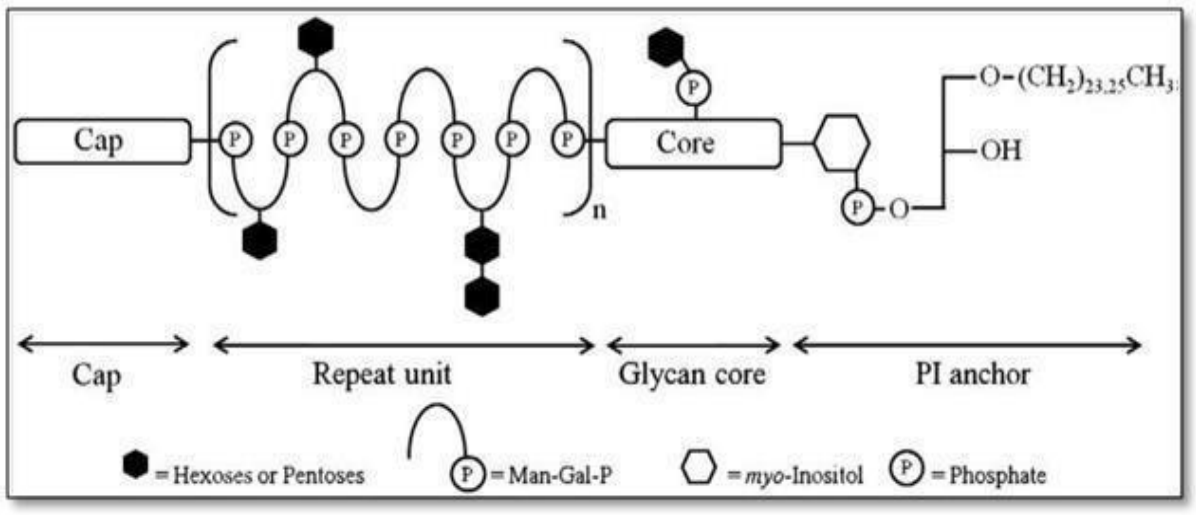

Figure 1.9: Leishmania LPG structure illustrating the four domains: conserved phosphatidylinositol-linked lyso-alkylglycerol lipid anchor and glycan core (GPI); and variable phosphorylated disaccharide repeats and cap structure. Adapted from (85)

The structure of LPG exhibits interspecies polymorphism variations among *Leishmania* species, determined by the number and type of phosphorylated oligosaccharide repeats (Figure 1.10) (85). Moreover, within the same species, the LPG structure undergoes changes as the parasites differentiate from procyclic promastigotes to metacyclic promastigotes, indicating intraspecies polymorphism (40). Notably, the modified LPG in metacyclic promastigotes displays increased numbers of PG repeats and side-chain galactose residues, no longer binds this promastigote stage to the sand fly's midgut. This enables these parasites to swim freely, promoting parasite transmission (86).

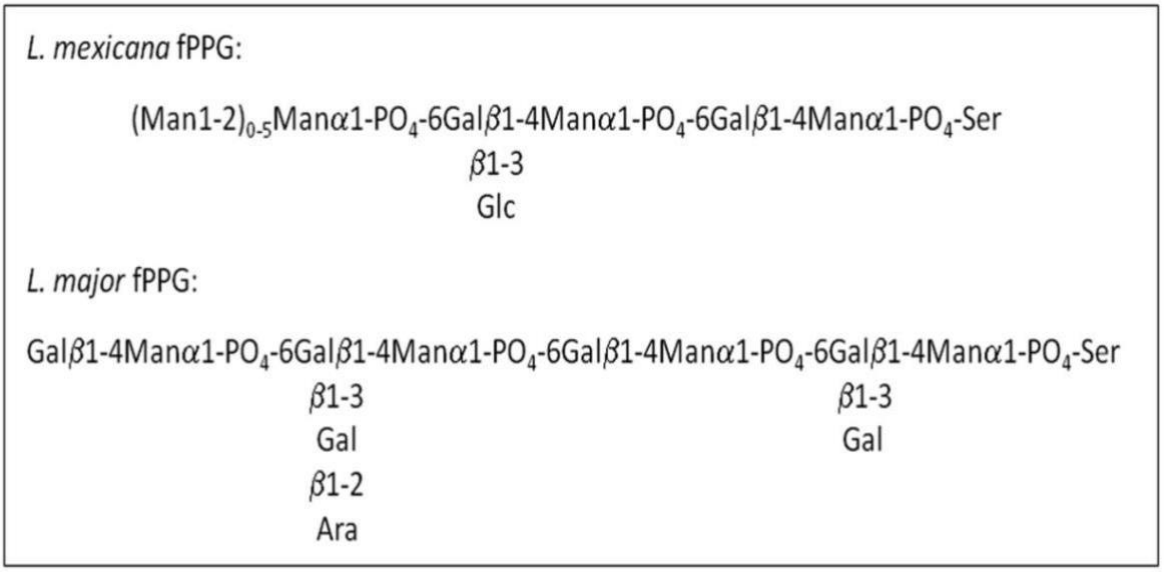

Figure 1.10: fPPG structures of different Leishmania species showing variations in the number of repeating units, sugar substitutions and cap structures. fPPG size 3- 6nm in diameter and upto 6 um in length. Adapted from (71)

LPG assumes additional roles in promoting infection following the invasion of the mammalian host. One crucial function is its ability to shield promastigotes from lysis by complement proteins (87). This protective role is particularly significant for procyclic promastigotes, as their susceptibility to lysis is attributed to their LPG structure, which contains half the number of repeating units compared to those observed in metacyclic promastigotes (88).

Furthermore, LPG serves as a vital ligand during the attachment of parasites to macrophage membranes. It achieves this by binding to other proteins, such as mannosefucose, expressed by macrophages (87,89). This interaction is pivotal for the establishment of infection and highlights the multifaceted role played by LPG in the intricate dynamics of *Leishmania*-macrophage interactions (87,89).

Gp63, another abundantly expressed surface protease molecule (90), plays multiple crucial roles in the survival and spread of the *Leishmania* parasite. Firstly, it imparts resistance to complement-mediated lysis, contributing to the parasite's ability to evade immune defences (71). Gp63 is also instrumental in facilitating the engulfment of the parasite by macrophages, a pivotal step in the establishment of infection. Moreover, gp63 plays a role in the activation of protein tyrosine phosphatases, resulting in the alteration of major signalling pathways (73,91). This ability to modulate signalling pathways is significant in the context of inhibiting microbial signalling, contributing to the parasite's enhanced survival and dissemination. Additionally, gp63 has the capability to downregulate host macrophage protein synthesis, further emphasising its intricate involvement in manipulating host cellular processes (59). The diverse functions of gp63 underscore its importance in orchestrating mechanisms that promote *Leishmania* survival and proliferation within the host.

1.2 The role of promastigote secretory gel (PSG) in leishmaniasis

1.2.1 The composition and structure of PSG

Sand flies containing mature *Leishmania* infections exhibit a distinctive phenomenon where their anterior midguts are obstructed by a 3D matrix gel, identified as the PSG (71,92). The primary component of PSG is fPPG (91), a mucin-like molecule that is unique to *Leishmania* parasites. fPPG is characterised by its extensive glycosylation and is a large, highly glycosylated, serine-rich LPG-like molecule comprised of [Gal- Man-PO(4)] repeats with a terminal cap structure linked to a serine-rich protein backbone. The notable phosphoglycosylation prevents the formation of secondary structures, imparting fPPG with its characteristic thread-like appearance (see Figure 1.11). Similar to LPG phosphoglycans, side sugars in fPPG can be variably substituted (93). Notably, research has shown that fPPG is produced by a diverse range of *Leishmania* species in culture as well (44).

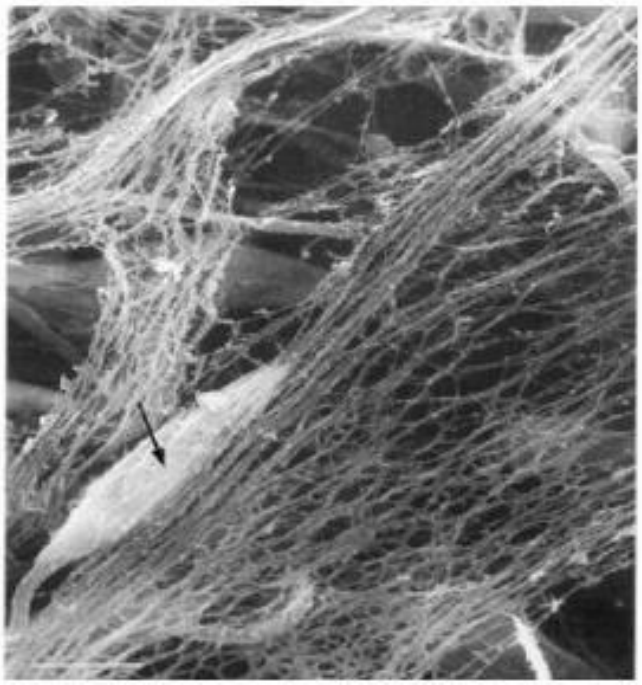

Figure 1.11: The fPPG meshwork containing entrapped promastigote (arrow) (SE image; Scale bar=2µm). Image by Stierhof et al. Adapted from (94)

1.2.2 Evidence suggesting PSG is secreted by leptonomad promastigotes

PPG has been detected in the guts of *L. longipalpis* infected with *L. mexicana* or *L. infantum* from day 2 to 3 onwards, with a notable increase in production observed from days 5 to 7 post-infection (95,96). This timeframe aligns precisely with the peak appearance of leptomonad promastigotes, strongly suggesting their involvement in PSG secretion. However, the specific cues initiating PSG production remain unknown. Nevertheless, there appears to be an intricate link between metacyclogenesis and PSG production in sand flies (55).

Scanning electron microscopy (SEM) has enabled the in-situ visualisation of the PSG plug, as depicted in Figure 1.11. Research utilising this technology has revealed that the cells within the implanted plug exhibit minimal movement and appear to be relatively inactive. However, when the PSG plug is placed in a culture medium, the PSG dissolves, and the parasites regain motility (61). Notably, the liberated promastigotes predominantly consist of leptomonad promastigotes, providing crucial evidence supporting the notion that PSG is secreted by leptomonad promastigotes (61).

1.2.3 Wound healing properties of PSG

PSG has demonstrated the ability to promote alternative macrophage activation and expedite wound healing in mice (97). These findings not only contribute valuable insights into the understanding of PSG's biological effects but also pave the way for potential therapeutic exploration. The observed effects suggest that PSG could be a promising target for future studies aimed at developing therapeutic interventions. Further investigation into the mechanisms by which PSG influences macrophage activation and wound healing could open avenues for novel treatment strategies in the context of *Leishmania* infections.

1.2.4 Role of PSG in *Leishmania* transmission

Recent research in leishmaniasis vector biology (59,79,93) have focused on determining the role of PSG in *Leishmania* transmission. The following two sections highlight and look into two roles of PSG in the transmission of *Leishmania.*

1.2.4.1 Manipulation of blood feeding behaviour

During blood feeding, the PSG plug serves a crucial role in the transmission dynamics of *Leishmania*. Specifically, the PSG plug exerts pressure on the stomodeal valve, ensuring that it remains open (71,93). This mechanism facilitates the regurgitation of saliva, secretions, and parasites along with the blood meal during sand fly feeding. The coordinated action of the PSG plug on the stomodeal valve is integral to the successful transmission of *Leishmania* parasites.

Additionally, the activity of parasite chitinases further contributes to the disruption of the stomodeal valve (74). This enzymatic action results in damage to the valve, exacerbating its malfunction and leading to a reduction in blood intake during subsequent feedings. The combined effects of PSG and parasite chitinases highlight the intricate strategies employed by *Leishmania* parasites to optimise the transmission process within the sand fly vector.

The presence of the PSG plug significantly alters the feeding behaviour of sand flies by obstructing their midgut, creating challenges for the parasite to obtain a blood meal (Figure 1.12) (98). Consequently, sand flies with the PSG plug spend an extended period feeding to acquire a sufficient blood meal due to the obstruction. Additionally, these insects are known to engage in more frequent biting attempts to overcome the hindrance, thereby enhancing the transmission of *Leishmania* parasites (93). This phenomenon is commonly referred to as the "blocked fly hypothesis" (98).

Furthermore, the regurgitation of metacyclic promastigotes during a blood meal results in the delivery of a higher number of parasites compared to inoculation alone with the proboscis, thereby further amplifying the transmission process (71,99).

The success of parasite transmission is contingent upon the timing of their introduction into the mammalian host. If the delivery occurs too early, there may not be a sufficient number of metacyclic promastigotes. Conversely, a late delivery could lead to sand fly susceptibility to the infectious pathogenic effects. Sand flies exhibit increased feeding persistence during the optimal time for transmission, highlighting the intricate interplay between the parasite and the vector in the transmission cycle (100).

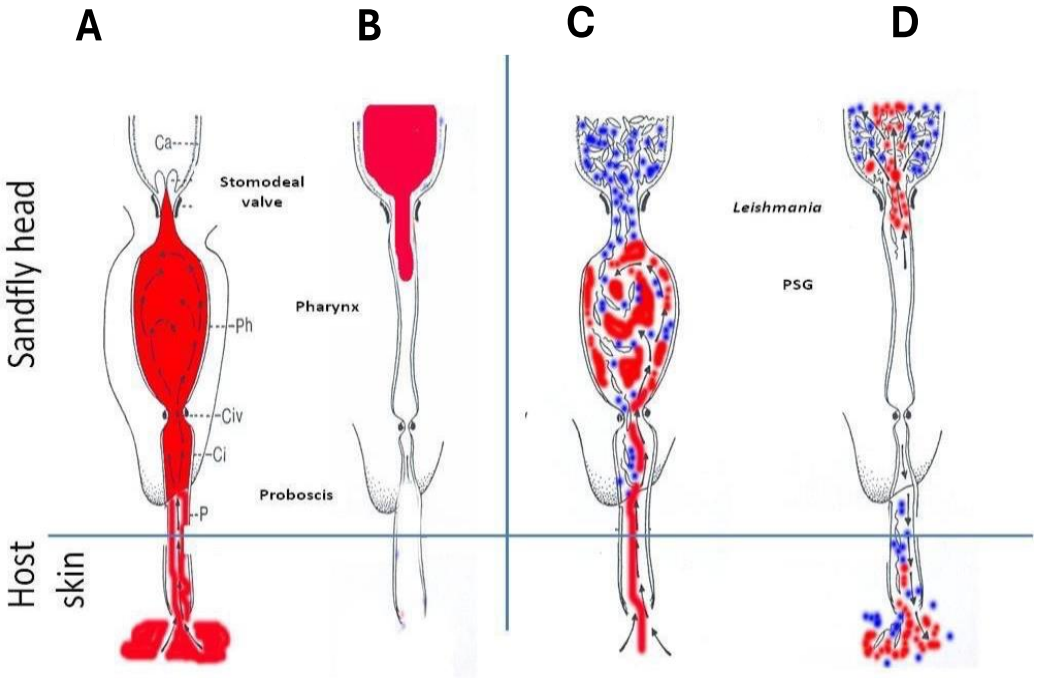

Figure 1.12: Regurgitation of parasite by sandfly during pool feeding: uninfected females (A&B) and infected females (C&D). Blood (red) and PSG (blue). Adapted from (71)

1.2.4.2 PSG and immunomodulation

Studies have revealed that the PSG, along with saliva, plays a pivotal role in promoting the recruitment of neutrophils and macrophages, thereby increasing the number of *Leishmania* host cells at the site of infection. Furthermore, PSG has been shown to elevate macrophage arginase activity, leading to an alternate activation of macrophages. This alteration in activation status enhances arginine metabolism, creating a favourable environment for parasite proliferation (101).

The consequence of this metabolic shift is a reduction in the availability of nitric oxide synthase, impeding the conversion of arginine into nitric oxide—a potent compound with parasite-lethal properties.

In addition to PSG, saliva has also been identified as a factor capable of inducing an alternate macrophage response (78). Due to their immunomodulatory properties, both PSG and saliva are being explored as potential vaccine candidates. Encouragingly, positive results have been observed in studies evaluating the immunogenicity and protective efficacy of these substances as potential components of leishmaniasis vaccines (102,103). The research in this area highlights the potential of PSG and saliva as immunomodulatory agents that could be harnessed for developing effective preventive measures against *Leishmania* infections.

1.2.5 Biological significance of motility

The importance of motility in the development of the parasite within the insect vector and subsequent infection of the mammalian host has been well-established in research (104,105). This study specifically focuses on the motile procyclic and metacyclic promastigotes of *L. mexicana*. Notably, metacyclic promastigotes were identified by Roger et al. (59) to be located within the anterior plug of the PSG rather than freely in the midgut. This finding aligns with earlier observations by Lawyer *et al.* (106) and Saraiva *et al.* (107), suggesting that metacyclic promastigotes possess the ability to move freely and swim across the PSG. Figure 1.13 depicts the parasite within the insect's mouthparts, emphasising its motile nature during this stage of the life cycle.

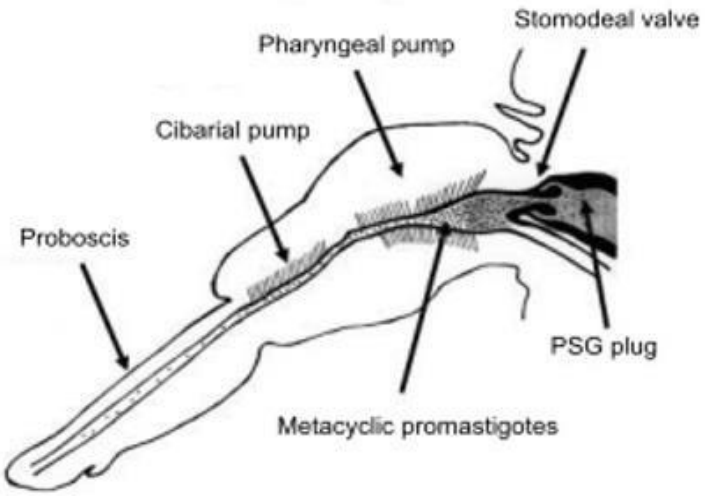

Figure 1.13: Sand fly mouthparts containing metacyclic promastigotes. Adapted from (61)

Procyclic promastigotes, in contrast to metacyclic promastigotes, have a distinct localisation within the sand fly. They are restricted to the PM in the abdominal midgut. During defecation, these parasites are expelled along with the blood meal. An alternative pathway involves their differentiation into nectomonad promastigotes, providing them with the capability to escape the PM. Consequently, procyclic promastigotes typically do not come into contact with the PSG.

To gain a better understanding of how environmental factors, specifically viscosity, influence the motility of these unique parasite forms, this study aims to investigate the motility of both procyclic and metacyclic promastigote cells across a range of viscosities. Recognising the impact of viscosity on motility is crucial, as it plays a vital role in the development and survival of the parasite. The research seeks to provide insights into whether the motility of *Leishmania* procyclic and metacyclic promastigotes is optimised for a specific viscosity. By comparing the parasite's swimming ability in PSG, a biologically relevant environment, the study aims to derive meaningful conclusions from the findings.

1.3 Study of *Leishmania mexicana* motility

1.3.1 Use of polymers in the study of *Leishmania* motility

PSG is identified as a mucin-like molecule (71). However, utilising commercial mucin for research purposes presents several challenges, such as the inherent variability in its mechanical properties across different batches, thereby compromising reproducibility. Additionally, acquiring PSG in sufficient quantities for investigation is a time-consuming and labor-intensive process.

Considering this, it is proposed that well characterised polymers be used to compare relative qualities, that is their unique attributes in respect to each other. Polymers are defined as large macromolecules formed by the chemical bonding of smaller molecules, or repeating units, called monomers (108). The polymers we used in this study are Ficoll and Polyvinylpyrrolidone (PVP)**.** These are highly characterised polymers (109). This choice aims to mitigate the challenges associated with the variability of commercial mucin and expedite the research process by utilising polymers with known and consistent properties (109).

1.3.1.1 Ficoll and Polyvinylpyrrolidone (PVP)

Ficoll, a synthetic, neutral, and highly branched polymer, is formed through the combination of sucrose and epichlorohydrin (Figure 1.14a). Its viscosity increases as more Ficoll is dissolved in a fixed volume of liquid, allowing for the examination of how the parasite is affected by different viscous properties (55). In this study, Ficoll PM400® with a molecular weight of 400 kDa was utilised. Ficoll has a long history of use in forming density gradients for the separation and isolation of eukaryotic cells. Due to its high molecular weight and low dialysable material content, Ficoll exhibits lower permeability towards cell membranes than sucrose. Consequently, cells are expected to collect at a lower density in Ficoll gradients compared to sucrose gradients.

The low membrane permeability and osmotic pressure of Ficoll contribute to better preservation of cell function and morphology. Ficoll has found applications in nucleic acid hybridisation, electrophoresis, and immunological studies (110).

Polyvinylpyrrolidone (PVP), another soluble, linear, and synthetic polymer, is composed of repeating N-vinylpyrrolidone monomers, forming a loose network (Figure 1.14b). Both the viscosity and elasticity of PVP increase with higher concentrations, making it suitable for examining how the parasite responds to viscoelastic properties (55). In this study, PVP360 with a molecular weight of 360 kDa was used. PVP serves various functions in cosmetic formulations, acting as a binder, emulsion stabiliser, film former, hair fixative, and non-surfactant suspending agent. Notably, PVP has been incorporated into iodine to create povidone-iodine, known for its disinfectant qualities. In molecular biology, PVP is utilised as a blocking agent during southern blot analysis (111).

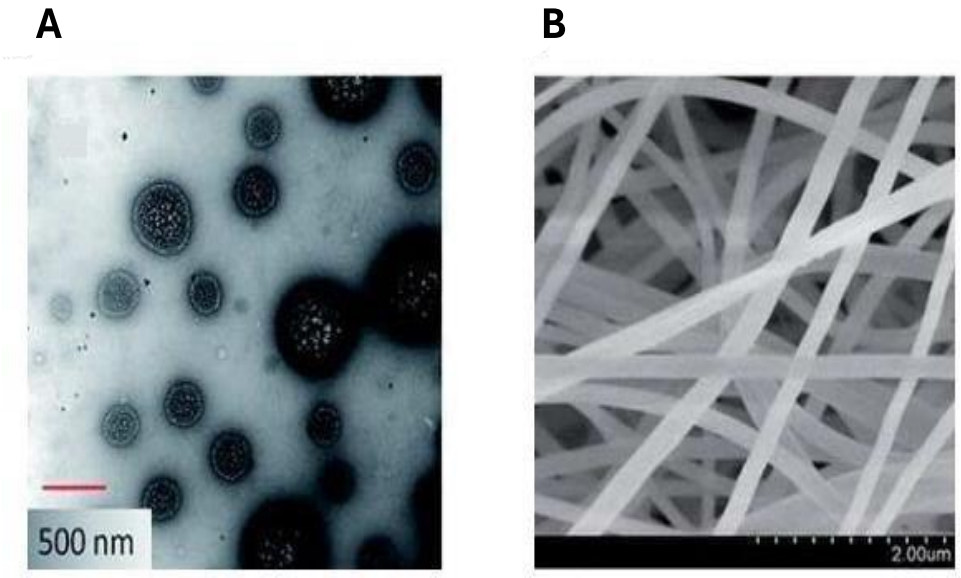

Figure 1.14: (A) Transmission electron micropgraph of Ficoll (112) (B) Scanning electron micrograph of PVP. Adapted from (113)

The investigation of *Leishmania* motility in both viscous (Ficoll) and viscoelastic (PVP) environments holds significance, as it remains uncertain which of these better represents the natural response of PSG (55). This study aims to shed light on the motility dynamics of *Leishmania* parasites in these distinct polymer-based environments, providing valuable insights into how the parasites navigate conditions that mimic aspects of the natural environment within the sand fly vector.

1.3.2 Mechanism and study of parasite motility

1.3.2.1 Reynolds number

Parasites and other microorganisms live in a fluid environment. Reynolds number is a useful parameter that enables us to project flow patterns in fluids. It is represented by the formula below:

$$Re = \frac{inertia\ forces}{viscous\ forces} = \frac{\rho.U.D}{\mu}$$

Where Re represents Reynolds number, ρ represents fluid density, D represents the dimensions of the object of interest, u represents the fluid velocity and μ represents the fluid dynamic viscosity (55).

In the case of human swimming, the Reynolds number is relatively high at $10^{4.}$ This indicates that the ratio of inertia forces to viscous forces is high, and inertia forces play a significant role. In contrast, microorganisms like bacteria operate in a much lower Reynolds number range of 10^{-4}, where viscous forces dominate, and inertia forces become negligible. In such microscopic environments, friction is the primary relevant force, and the active movement of microorganisms relies on the drag force generated by structures like oscillating flagella (55). Understanding the Reynolds number helps provide insights into the predominant forces at play in different fluid environments and their implications for the movement and behaviour of organisms within them.

Microorganisms have evolved various propulsion mechanisms to navigate and exploit their fluid environments, effectively overcoming viscous drag (55). A crucial aspect of this propulsion is the non-reciprocal movement, achieved by generating lateral displacement waves along their flagella (55). Different microorganisms employ distinct strategies for this purpose. *Escerichia coli* and other bacteria use a rotating flagellum in a corkscrew pattern to achieve propulsion. Human sperm cells adopt a helical waveform of a single flagellum, deforming planar swimming patterns. *Chlamydomonas spp.* use asymmetric power and recovery strokes of their two flagella. Belonging to the same family as *Leishmania*, trypanosomes are pulled forward by the planar beat of their flagella and leverage their asymmetrical body shape to induce rotational motion. While these propulsion strategies are well documented for various microorganisms, the specific details of the strategy employed by *Leishmania* remain unknown at present (55). Investigating and understanding the propulsion mechanisms of *Leishmania* is essential for comprehending its movement within the host and vector environments, contributing to broader insights into parasitic behaviour.

The findings from studies on trypanosomes are intriguing as these indicate faster microbe swimming speeds in viscoelastic environments like blood or collagen networks (114). Additionally, the observation that trypanosomes swim faster in pillar arrays compared to a purely viscous culture medium, utilising the suspended obstacles for propulsion, adds another layer of complexity to their swimming patterns (114). Given these insights into the swimming behaviour of trypanosomes in different environments, it indeed raises an interesting question about whether *L. mexicana* cells exhibit similar trends. Investigating the swimming patterns of *L. mexicana* in viscoelastic environments could provide valuable information on how these parasites navigate within the vector, offering insights into the adaptations and strategies employed by *Leishmania* during different stages of its life cycle.

1.3.2.2 Methods used in the study of parasite motility

Our understanding of parasite motility is limited to the available methods that can be utilised for study. Various technologies have been employed in the past to investigate motility, including high speed videomicroscopy, light sheet fluorescence microscopy, real time confocal microscopy, high speed fluorescence microscopy, differential interference contrast microscopy, and differential dynamic microscopy (55). While these techniques have contributed significantly to our understanding of parasite motility, it is important to acknowledge the drawbacks associated with each method. For example, although differential dynamic microscopy is a quick method, it only characterises a limited number of motility parameters (115).

Recent technological advances have indeed revolutionised our ability to track and image microorganisms, providing valuable insights into their behaviour. The development of three-dimensional (3D) methods for studying parasite motility has been particularly impactful in enhancing our understanding of these organisms. For example, 3D methods have been employed to track the trajectories of *T. brucei*, revealing distinct swimming states such as swimming and tumbling (116). One notable technique in this context is digital inline holographic microscopy, a high- throughput 3D method extensively used to study motility in various microorganisms, including bacteria and sperm (117,118). This method could be instrumental in investigating *Leishmania* motility, offering the capability to capture and analyse the 3D movement of these parasite cells (55).

Understanding how *Leishmania* cells move during critical phases of their lifecycle, especially during transmission, can provide crucial insights and potential intervention points for controlling the spread of leishmaniasis. The application of digital inline holographic microscopy to *Leishmania* research holds promise for advancing our knowledge of parasite motility.

1.3.2.3 Digital Inline Holographic Microscopy (DIHM)

The introduction of digital inline holographic microscopy (DIHM) approximately 2 decades ago marked a significant advancement in the field of parasite motility (119). DIHM enables 3D imaging of microscopic samples, offering a quick and non- intrusive method for studying the movements of microorganisms in diverse environments. This technology facilitates the investigation of how variables such as temperature, viscosity, and chemical stimuli impact the swimming behaviour of microorganisms (99).

DIHM presents several advantages. Notably, it eliminates the need for sample preparation steps like staining, allowing for the rapid visualisation of living cells. A single hologram contains comprehensive data related to the parasite's 3D structure, and free software for data post-processing is readily available. However, there are certain drawbacks associated with the use of DIHM. Health and safety concerns arise from the technology's use of lasers, and without proper interlocks, microscopes can concentrate relatively low-power laser light to dangerous levels (99).

In summary, DIHM remains a powerful tool for studying microorganisms' motility and structure, providing valuable insights into their behaviour and responses to environmental factors. Its application to *Leishmania* motility research holds promise for enhancing our understanding of the intricate movements of these parasites.

a) Principle of holography

The foundational principle of holography involves the interference between two waves. In holography, a light wave scattered by an object of interest (referred to as the object wave) is combined with a wave possessing a known phase (known as the reference wave). When the electric fields of these object and reference waves intersect, they create an interference pattern characterised by alternating light and dark fringes, representing constructive or destructive interference (120).

Indeed, the key characteristic of holography that distinguishes it as "inline" holographic microscopy is that both the object and reference waves travel along the same path through the imaging system (120).

b) Optical setup

Two configurations for an inline holographic microscope are illustrated in Figures 1.15a and 1.15b, featuring different lighting setups. Figure 1.15a depicts a configuration utilising LED (light-emitting diode) as a light source, while Figure 1.15b displays an illumination system incorporating a laser connected to a single- mode optical fibre. The use of a laser, due to its high intensity, eliminates the need for collimation and, consequently, does not require a condenser lens in this setup (121).

These setups employ varying degrees of optical coherence, a property that determines the ability of the object wave to deviate from the reference wave and still generate interference fringes. An LED source, possessing low inherent coherence, necessitates a 'pinhole' condenser aperture to introduce a minimal level of coherence. Holography using an LED requires a small optical path length difference between the reference and object waves to produce fringes, limiting the thickness of the sample volume that can be captured at once, as indicated by the red-highlighted region in the lower panel of Figure 1.15a. In contrast, the high coherence of a laser allows for the photography of significantly thicker sample volumes at both high and low magnifications, expanding the "sensitive volume." A downside is that it can also introduce unintended contributions such as dust particles and defects on the sample chamber's surface into the optical path during experiments (121). Figure 1.15b displays the optical arrangement utilised in this research study, leveraging the laser's capacity to sample large volumes. During post-processing, measures were taken to eliminate undesirable resultant noise.

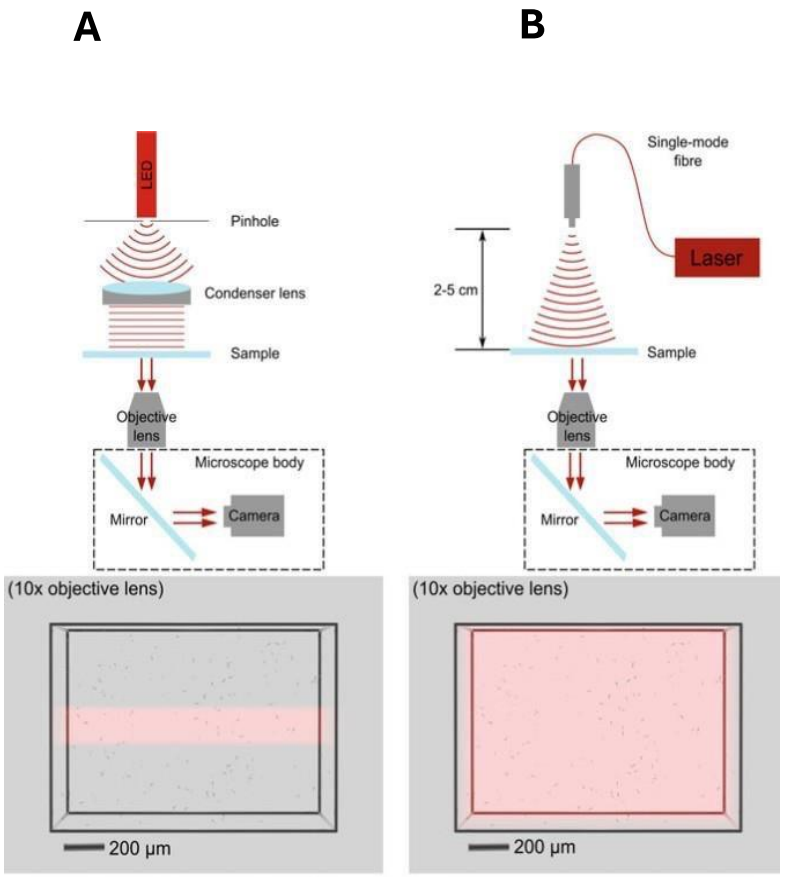

Figure1.15: Layouts for digital inline holographic microscopy (DIHM) (121)

c) Data processing

Raw DIHM photos in 2D (two dimensional) resemble out-of-focus microscope photographs. These photos contain 3D positions and shapes of the cells in the sample chamber. Holographic images can be computationally processed to get 3D information using various methods (122,123). The most practical computing method to use for 3D localisation of weakly scattered objects is the Rayleigh-Sommerfield back-propagation system because it is rapid and adaptable (124). Holographic images are treated as planes in 3D space. It considers each pixel in the raw image to be a source of light wave with the same phase, and amplitude set by pixel values. (A light pixel is a strong source; a dark pixel is a weak source.) It is then possible to "numerically refocus" the raw image at an arbitrary distance within the sample by summing the contributions from all sources at a certain position across a plane parallel to the holographic image (120). Typically, this technique yields a stack of photos that mimics manually moving the microscope's focus plane through a sample and capturing pictures at various depths (121).

The holographic recording and reconstruction process generates data that may be evaluated at a range of length scales. Previously, researchers either performed high-resolution single-cell shape analysis or determined the "centroid" position of a cell and tracked it over time (123). This study used the latter way to learn more about cell swimming patterns, which entails tracking each cell concurrently across several frames at low magnification and high video frame rates.

d) DIHM applications

Utilising DIHM, individual cell locations can be simultaneously tracked across various frames at low magnification and high video frame rates. This approach provides valuable information on the swimming patterns of cells, shedding light on how they colonise new territory, interact with each other, and respond to their environment (55). In this specific study, DIHM was employed to track the movement of individual *L. mexicana* parasite cells in different viscosities, yielding 3D displacement information that contributes to a better understanding of their swimming mechanisms.

1.3.2.4 Swimming trajectories of *L. mexicana*

Describing 3D trajectories involves considering parameters such as helicity. These metrics are useful for characterising the swimming patterns of *L. mexicana* promastigote cells, especially since they navigate in 3D. Analysing these parameters provides insights into the intricate movements and behaviours of the parasites during their swimming phases.

a) Velocity

Velocity is defined as a change in position over time. Since parasites move, their instantaneous velocity may be calculated (rate of change of position with respect to time interval which is very small) (125). As illustrated in the formula below, this can be determined from individual positions P (t) by dividing displacement by time (t):

$$V(t) = \frac{P(t+\Delta t) - P(t)}{\Delta t}$$

b) Curvature and torsion

Curvature is the measure of how much a curve deviates from being a straight line. In the context of *Leishmania* motility, curvature can provide insights into the degree of bending or turning in the trajectory of the parasite. Torsion, on the other hand, is the degree of twisting or rotation along the length of a curve. It helps to understand the rotational aspects of the trajectory.

The Frenet-Serret formulas play a crucial role in describing the geometric properties of a curve in 3D. These formulas involve the concepts of tangent (T), normal (N), and binormal (B) vectors, and they are employed to calculate the curvature (κ) and torsion (τ) of a curve. The Frenet–Serret formulas are:

$$\frac{dT}{dS} = \kappa N$$

$$\frac{dN}{dS} = -\kappa T + \tau B$$

$$\frac{dB}{dS} = -\tau N$$

Where $\frac{d}{ds}$ is the derivative with respect to arclength, κ is the curvature, and τ is the torsion of the curve. The tangent vector (T) represents the direction of motion along the curve. The normal vector (N) points towards the centre of curvature, providing information about how the curve is bending. The binormal vector (B) is orthogonal to both the tangent and normal vectors, defining the twisting or rotational behaviour of the curve (126). These mathematical tools are valuable for quantifying the intricate motion of *Leishmania* parasites in 3D (55).

c) Chirality and helicity

Chirality refers to the property of asymmetry in a molecule or object that is not superimposable on its mirror image. The chiral centre of a molecule is the point at which chirality is present or absent in that molecule (127). Helicity is the property of having a twisted, helical structure. This is also referred to as innate chirality. However, this asymmetry is caused by the twisted 3D structure rather than chiral centres (127). By evaluating these asymmetry-related traits, we may determine whether the cells are more likely to travel in a clockwise or anticlockwise helical pattern.

1.3.3 *Leishmania mexicana* motility studies using 3D imaging

The study conducted by Findlay *et al.* (128) provides valuable insights into the distinct swimming patterns exhibited by *L. mexicana* procyclic promastigote and metacyclic promastigote cells. Metacyclic promastigote cells were observed to swim in a "run and tumble" pattern (Figure 1.16a). This type of motion is characterised by a period of relatively straight swimming (run) followed by a sudden change in direction (tumble). It is characteristic of microbial sensing of stimulus in the environment. In the presence of macrophages, metacyclic promastigote cells were capable of modifying their swimming direction and speed (128). This adaptive behaviour suggests an ability to respond to the presence of host immune cells. Procyclic promastigote cells exhibited a different swimming pattern compared to metacyclic promastigotes. They were described as swimming more slowly and in a meandering helical pattern (128) (Figure 1.16a). The illustration in Figure 1.16b visually represents the dominant swimming phenotypes of procyclic and metacyclic promastigote forms of the parasite. These findings highlight the dynamic and adaptive nature of *L. mexicana* metacyclic promastigote cells in response to their microenvironment, particularly in the presence of immune cells. The ability to exhibit different swimming patterns may play a crucial role in the parasite's survival and host interactions.

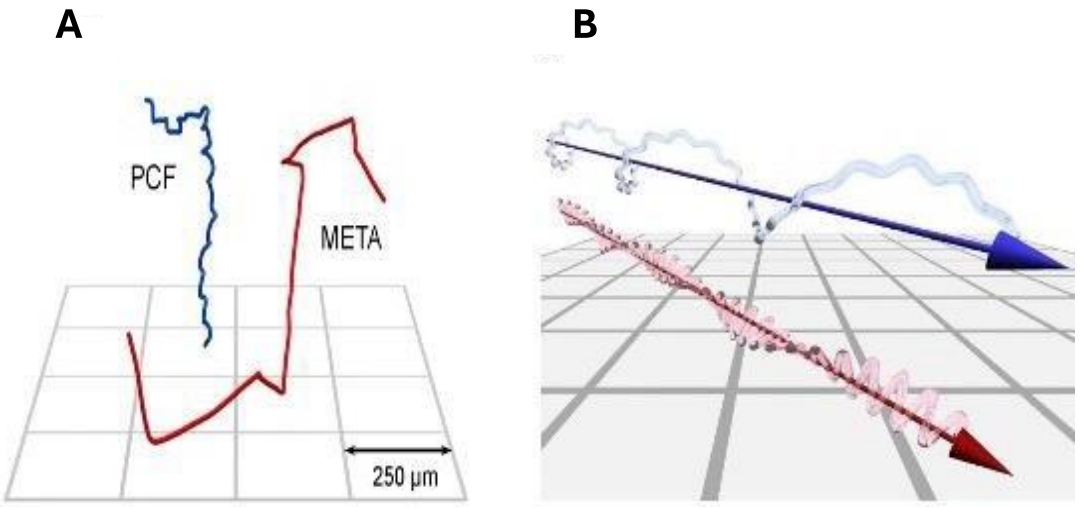

Figure 1.16 (A) Single cell track of procyclic (PCF) and metacyclic (META) cell. (B) Cell tracks illustrating dominant swimming phenotype for PCF (Blue) and META (Red). Adapted from (128)

1.3.4 Use of magnetic tweezers to determine polymer viscosity

Magnetic tweezers (MT) serve as a valuable tool for studying the mechanical properties of complex fluids, particularly in cases where sample availability is limited, such as in the study of substances like PSG (129). There are two main designs of magnetic tweezers: vertical and horizontal, both of which share a common principle (130) and are suitable for various applications.

The fundamental concept behind MT involves actively manipulating a small particle (microscopic) within a sample by applying a known force or displacement, and then measuring the particle's reaction. This process provides information about the rheology of the embedding medium, including its viscosity (129).

The key components of MT setup include coils which are typically wound around an iron core to generate the magnetic field essential for manipulating the magnetic microparticles. This is then mounted on a microscope stage which allows for precise positioning and observation of the sample under a microscope.

The molecule of interest is attached to a magnetic microparticle (probe). The probes that are typically used are paramagnetic, super-paramagnetic or ferromagnetic beads (129). These beads have a high uniformity in size and shape, thus allowing for reproducibility of results (130).

The entire process, including the movement and response of the magnetic microparticles, is monitored and recorded using a microscope and connected laptop. By manipulating the microbeads and measuring their response, researchers can measure mechanical properties of the sample, including viscosity. In the context of studying PSG, MT provides a means to understand the rheological characteristics of this complex fluid.

The force (F) on a magnetic moment (m) due to a magnetic field (B) is given by the equation:

$$F = (m.\nabla) B$$

This equation tells us that the more the magnetic particles, the stronger the magnetic field. Calculation can be used to determine the force exerted by the magnetic field on the magnetic beads. Force calibration will be required. The viscous drag of the microbeads can be used as a force calibration method.

We know that the microbeads are being dragged through a viscous medium (Newtonian fluid of known viscosity η) while their position is being recorded. They exhibit Brownian motion. Since the Reynolds number for the system is low, and we already know the particle radius as well as velocity *v* (we can determine velocity using the recorded velocity values), we can apply Stoke's equation to determine the resistance force applied:

$$F = 6\pi a \eta v$$

MT are valuable tools in studying the mechanical properties of biological materials. Their simplicity, low cost, and versatility make them accessible for a range of applications. The limitations in temporal and spatial resolution, often associated with data gathering through video microscopy, can be addressed by incorporating high-speed cameras, enhancing the capabilities of MT (131).

New designs, such as magnetic torque tweezers and electromagnetic torque tweezers, have expanded the capabilities of traditional magnetic tweezers. These advancements contribute to a more comprehensive understanding of the physical properties of biological materials. Additionally, other powerful tools like optical tweezers and atomic force microscopes further complement the study of biological materials, providing researchers with a diverse set of techniques to investigate different aspects of cellular and molecular mechanics (132).

Magnetic spectroscopy's fast development and its broad applications in physics and biology highlight its significance as a technology with the potential to unravel complex biological processes and contribute to advancements in various scientific fields. As technology continues to evolve, researchers can leverage these tools to delve deeper into the intricacies of biological systems.

1.3.5 Reverse transcription poly*m*erase chain reaction (RT-qPCR) and cell stage validation in *Leishmania*

Reverse Transcription Polymerase Chain Reaction (RT-PCR) is a molecular biology technique commonly used for RNA detection and quantification. It involves reverse transcription of RNA into complementary DNA (cDNA) followed by PCR amplification. Quantitative RT-PCR (RT-qPCR), a real-time variant, allows real-time monitoring of the amplification process. RT-qPCR finds use in gene expression analysis, RNA validation, pathogen detection, genetic testing, and disease research (133). In leishmaniasis research, RT-qPCR has been crucial for diagnostic purposes.

This study used RT-qPCR to molecularly validate metacyclic and procyclic promastigote cell stages of *L. mexicana* using stage-specific mRNA markers; *sherp* (Small hydrophilic endoplasmic reticulum associated protein*)* and *histone h4* (*hh4*). Using *nmt* (N-myristoyltransferase) RNA as a standard reference provided a stable baseline for comparison, as its expression remains constant. Overall, RT-qPCR serves as a powerful and precise molecular tool in the investigation of gene expression and cellular processes, offering valuable insights into the dynamics of *Leishmania* parasite stages.

1.3.5.1 Choosing between one and two step RT-qPCR

RT-qPCR can be performed through either a one-step or a two-step assay, each with distinct advantages and limitations. One-step assays involve combining reverse transcription and PCR in a single tube (134). This approach offers advantages in terms of speed and reproducibility, as both reactions occur in the same tube, minimising experimental variation and contamination risks. However, one-step assays are less sensitive compared to two-step assays and pose challenges in optimising the combined reactions separately. In contrast, two-step assays separate the reverse transcription and PCR processes into different tubes, each with optimised buffers, conditions, and priming strategies (134). They produce a stable cDNA pool that can be stored for extended periods and used for multiple reactions. However, the use of multiple tubes increases pipetting steps and consequently risk of DNA contamination. This method is time-consuming and requires more optimisation than one-step assays. Researchers often choose between these approaches based on their experimental goals, considering the trade-offs associated with each method.

1.3.5.2 Selecting RNA for reverse transcription

When designing RT-qPCR, a crucial decision is whether to use total RNA or mRNA (messenger RNA) as the reverse transcription template. While mRNA offers slightly greater sensitivity, total RNA is often preferred due to significant advantages as a starting material.

Using total RNA requires fewer purification steps, leading to more quantitative template recovery and better normalisation of results to the initial number of cells. Additionally, by omitting mRNA enrichment steps, the risk of skewed data from varying recovery yields for different mRNAs is minimised (134). Ultimately, the choice between total RNA and mRNA as the RT-qPCR template depends on experimental goals, the need for sensitivity, and the desire to avoid biases introduced by enrichment stages.

1.3.5.3 Choice of primers

Four common primer approaches in two-step assays include oligo(dT) (deoxythymidine) primers, anchored oligo(dT) primers, random primers, and sequence-specific primers (Figure 1.17).

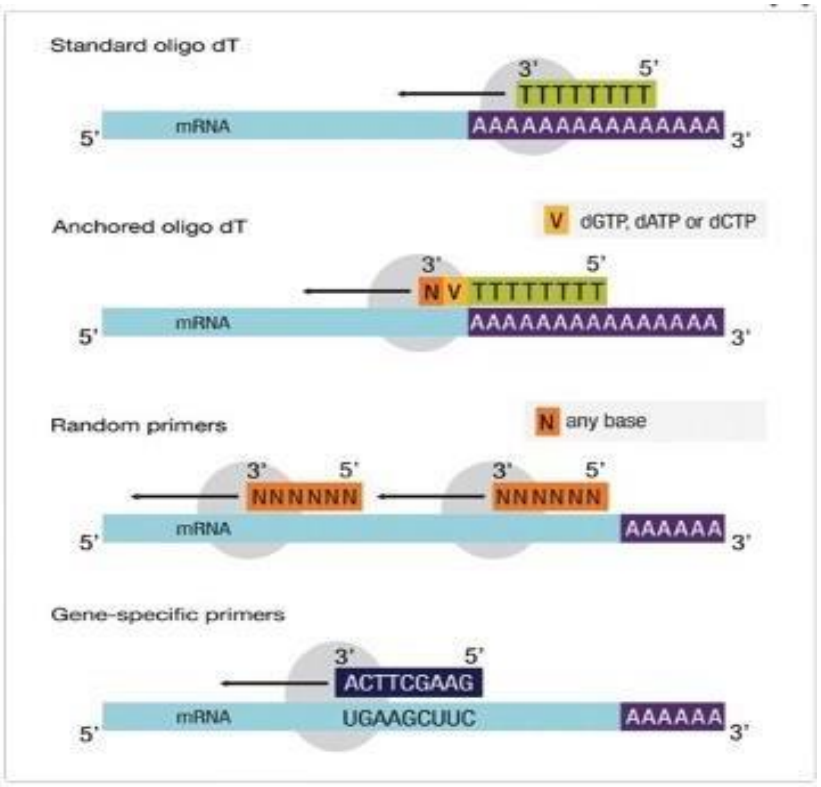

Figure 1.17: Types of primers. (134)

Oligo(dT) primers efficiently capture polyadenylated (poly A) mRNA from eukaryotic organisms but may miss non-polyadenylated RNA. Anchored oligo(dT) primers, with an additional anchor sequence, enhance specificity but still may overlook non-poly A RNA. Random primers, being 6 to 9 bases long, bind at multiple points along the RNA transcript, yielding high cDNA yield from various RNA types. However, they lack specificity for mRNA, potentially diluting mRNA signals and including unwanted sequences in the cDNA pool. Sequence-specific primers target specific mRNA sequences with high specificity but require prior knowledge of target sequences and exhibit a bias toward the 3' untranslated region (UTR) (134).

In summary, oligo(dT) and anchored oligo(dT) are suitable for polyadenylated mRNA, random primers can capture non-poly A RNA, and sequence-specific primers offer high specificity. Despite a 3' UTR bias, oligo(dT) primers were used in this study for their strong mRNA enrichment, aligning with the focus on validating the presence of specific *Leishmania* parasite cell stages using *sherp* and *histone h4* mRNA.

1.3.5.4 Designing primers

For the quantitative PCR (qPCR) stage of RT-qPCR, it is ideal to design primers that span the exon-exon junction, with one primer potentially spanning the actual exon- exon boundary (126). This design helps avoid amplification of intron-containing genomic DNA sequences, thereby reducing the risk of false positives from contaminating genomic material. To prevent genomic DNA contamination, RNA samples should undergo treatment with RNase-free DNase. Additionally, if it is challenging to design primers that separate exons or exon-exon boundaries, considering treatment with dsDNase may be a viable option (134).

1.3.5.5 Role of reverse transcriptase (RT) in RT-qPCR

Reverse transcriptase (RT) is an enzyme crucial for converting RNA into DNA during the reverse transcription step (132). The ideal RT should exhibit high thermal stability to enable cDNA synthesis at elevated temperatures.

This characteristic is essential for successful transcription of RNA with complex secondary structures, ensuring full activity throughout the reaction and leading to higher cDNA yields. In the study, Taq polymerase, derived from the thermophilic bacterium *Thermus aquaticus*, was used. Native Taq polymerase, however, has residual activity at lower temperatures, leading to undesired product formation. To address this, 'hot start' Taq polymerases, either antibody-blocked or chemically blocked, are used to prevent enzyme activity until the high-temperature denaturation step (134).

RNase H activity facilitates the degradation of RNA from RNA-DNA duplexes during cDNA synthesis, promoting efficient double-stranded DNA formation. In qPCR applications, RT with intrinsic RNase H activity is commonly used. This is advantageous as it contributes to melting RNA-DNA duplexes in the initial PCR cycles, enhancing the overall efficiency of the process (134).

1.3.5.6 Amplicon detection

Fluorescence technology is pivotal in amplicon detection during RT-qPCR, with probes incorporated into PCR mixtures to monitor DNA amplicon concentration changes. Two common probes are SYBR® Green I dye, specific to double-stranded DNA (dsDNA), and dual-labelled probes, known as hydrolysis or TaqMan® probes (135). SYBR® Green I dye, binding to dsDNA, produces signals that intensify as PCR progresses. In contrast, dual-labelled probes consist of a single-stranded oligonucleotide marked with a reporter dye and a quencher. Taq DNA polymerase's 5' exonuclease activity separates the reporter and quencher, producing a signal proportional to amplicon yield (135). Dual-labelled probes offer specificity and precision for low-copy-number targets but are costlier and require meticulous design. SYBR® Green I dye lacks specificity, binding indiscriminately to all products, posing challenges in accurate quantification. The use of a post-PCR melt curve analysis can aid in assessing reaction specificity (135).

Less frequently used probes include molecular beacons, recognised as hybridisation probes, as well as LightCycler and Scorpions® probes. Additionally, alternative fluorescent dyes like Ethidium Bromide or Acridine Orange can be utilised; however, SYBR Green is favoured for its elevated signal intensity (135).

In summary, RT-qPCR stands out as an advanced instrument for studies in parasite biology, offering advantages in terms of automation and high-throughput capabilities.

1.4 Aim and objectives

Although we know that motility is required for *L. mexicana* to survive, develop, and infect mammalian hosts, causing disease, there is limited research that explores how this parasite's external environment affects its motility. Thanks to recent advances in pertinent microscopy technology, we are able to track and quantify movements of *Leishmania* motile cells in 3D to learn how the parasites use swimming processes to overcome environmental constraints and continue to spread the disease. This research builds upon work by Findlay *et al*. (128) that described the distinct movements of motile metacyclic promastigote and procyclic promastigote cells of *L. mexicana*.

The specific objectives of this research are to:

1. To culture procyclic promastigote and metacyclic promastigote cells, harvest enriched populations of each lifecycle stage and validate these using a molecular method, RT-qPCR.

2. Capture and describe swimming patterns of both promastigote stages in Ficoll, PVP and fPPG in different viscosities using holographic microscopy.

3. Compare parasite swimming patterns in the context of differential polymer viscosity.

4. Determine the relative viscosity of Ficoll, PVP and fPPG using magnetic tweezers.

This study's findings will help us better understand *L. mexicana* motility and serve as a foundation for future disease management targets.

2 MATERIALS AND METHODS

2.1 Cell culture

L. mexicana wild type (strain M379) procyclic promastigote cells were cultured in M199 medium (pH 7.2) at 26°C (de Pablos *et al*) (136). M199 medium used was modified with 25nM HEPES, Hanks' Salts and L-glutamine (Gibco) and supplemented with foetal bovine serum, HEPES, penicillin streptomycin, adenine, and Hemin. This was consistent with previous studies (136).

All cells were maintained within low passage numbers (<4). On day 3, the procyclic promastigote cells were harvested at concentration between $3–6\times10^6$ cells/ml, mid-logarithmic phase and diluted to 10^4 factor into fresh M199 medium for holographic tracking.

To enrich for metacyclic promastigote cells, some of the harvested procyclic promastigote cells were passaged into Grace's medium (pH 5.5) at 2×10^5cells/mL and grown for 6 days at 26°C (de Pablos *et al*.) (136). Grace's medium used was modified with 0.6g/L L-Glutamine (Sigma), and supplemented with foetal bovine serum, BME vitamins, sodium bicarbonate and penicillin streptomycin. These cells were harvested at concentration between $2–5\times10^7$ cells/ml and placed atop a 10% ficoll gradient density centrifugation to size-isolate metacyclic promastigote cells (Späth and Beverley) (137). Size-isolated metacyclic cells were diluted to 10^4 factor into fresh M199 medium and Grace's medium for holographic tracking.

To remove parasite rosettes and obtain more accurate measurements on free individual parasite movements, both procyclic promastigote and metacyclic promastigote cells were passed through a Thermo Scientific™ blunt 23-gauge 10ml removable glass needle syringe prior to cell counting and dilution for holographic tracking.

Room temperature whilst conducting all the video capture was kept at 32°C to mimic host environment and avoid convection effect that occurs through heating only the microscope stage.

For motility analyses, samples of 1-3×10^7 cells were centrifuged in a Thermo scientific Heraeus™ bench top centrifuge at 2000g for 10 minutes and the supernatant was discarded. The resultant pellet was suspended in 300 µL of Trizol™ reagent (ThermoFisher Scientific) and stored in -20°C ready for RNA extraction using Direct-zol™ RNA prep kit (Zymo Research).

2.2 RNA extraction and molecular validation of L. mexicana promastigote stages using RT-qPCR

2.2.1 RNA extraction

For RNA extraction, an equal volume of 300 µL of absolute ethanol was added to the sample suspended in Trizol™ reagent (ThermoFisher Scientific), followed by vortexing. The mixture was then transferred to a Zymo Spin II column (Zymo Research) in a collection tube and centrifuged at 16,000g for 30 seconds. The eluate was then transferred to a new collection tube, and the supernatant was discarded. Pre-washing was conducted by adding 400 µL of Direct- zol™ RNA prewash (Zymo Research) to the column, followed by centrifugation at 16,000g for 30 seconds. This step was repeated for thorough pre-washing. Subsequently, washing was carried out by adding 700 µL of Direct-zol™ RNA wash buffer (Zymo Research) to the column and centrifuging at 16,000g for 1 minute. The column was then transferred to an RNA-free eppendorf tube, and 50 µL of DNAse/RNAse-free water was added. Afterward, centrifugation at 16,000g for 30 seconds was performed. The extracted and purified RNA was then kept on ice for further use.

2.2.2 RNA quantification and DNAse treatment

RNA quantification was conducted through spectrophotometry analysis by measuring absorbance at 260nm using a Thermo Scientific Nanodrop 1000 spectrophotometer connected to a laptop, where 1 µL of the sample was placed on the device arm, which was then lowered, and the resulting reading was recorded in ng/µL.

Routine DNAse treatment was carried out using the TURBO DNA-Free™ kit (ThermoFisher Scientific) to eliminate DNA, and RNA quantification was repeated. A solution comprising 5µl of 10X Turbo DNAse buffer, RNA (2µg), and 1µL of TURBO DNAse enzyme was incubated at 37°C for 25 minutes. Inactivation was performed by adding 2µL of DNAse inactivation reagent and incubating at room temperature for 5 minutes. The samples were then centrifuged at 10,000g for 1.5 minutes, and the supernatant containing RNA was carefully transferred to a fresh tube.

2.2.3 cDNA synthesis

First strand cDNA synthesis was performed using SuperScript™ II reverse transcriptase (RT) (ThermoFisher Scientific), with 10ng of RNA in a total reaction volume of 20µl. A solution was prepared by combining 1µL Oligo(dT) (500µg/mL), 1µL of mRNA, and 1µL of dNTP mix (10mM each), which was then adjusted to 12 µL using sterile distilled water. This mixture was heated to 65°C for 5 minutes, chilled, and the contents were collected by a brief centrifugation. To this, 5X first-strand buffer (4µL), 0.1M DDT (2 µL), and RNAse Out™ (40 units/µL) (1µL) (ThermoFisher Scientific), were added. The contents were mixed and incubated at 42°C for 2 minutes. Subsequently, 1µL (200 units) of SuperScript™ II RT (ThermoFisher Scientific) was added, and the solution was mixed by gently pipetting up and down. The incubation was carried out at 42°C for 50 minutes, followed by inactivation through heating at 70°C for 15 minutes.

2.2.4 PCR reaction

The reaction mixture for each sample was prepared by combining 10µL of Fast SYBR® Green Master Mix (2X) (ThermoFisher Scientific), forward and reverse primers, cDNA templates, and RNAse-free water in a tube. The contents were gently mixed by inversion, and the tube was centrifuged to eliminate air bubbles. The appropriate volume of each reaction was then transferred to a MicroAmp™ Fast Optical 96-well reaction plate (ThermoFisher Scientific), resulting in a total reaction volume of 20 µL. To achieve optimal performance, 20ng of cDNA was used per 20 µL reaction volume. Table 2.1 below lists primers that were used for the PCR reaction.

Primer name	Primer sequence (5' to 3')
*L mexicana_nmt*_qPCR_F	GCCAAAGACGGTGGCCGATA
*L mexicana_nmt*_qPCR_R	GGCGTCCACCACTCAAATGT
*L mexicana_Histone h4*_qPCR_F	TACTGAAGGCCTACGTGGAG
*L mexicana_Histone h4*_qPCR_R	AGCGCATTCACAACATCGG
*L mexicana_Sherp*_qPCR_F	AAGGGACCAGATGAGCAACG
*L mexicana_Sherp*_qPCR_R	CACCATCCTTCAGCTCCTGG

Table 2.1: Primers for PCR reaction. F represents forward primer and R represents reverse primer

The plate was sealed with an optically clear qPCR plate seal, briefly centrifuged, and then placed in the Quantstudio 3 PCR System (ThermoFisher Scientific). The reaction underwent an initial holding step at 95°C for 10 minutes, followed by an amplification step comprising 40 cycles of 95°C for 15 seconds and 60°C for 1 minute. A single dissociation step was carried out at 95°C for 15 seconds, 60°C for 20 seconds, and 95°C for 15 seconds. For negative control, DNAse free water was loaded instead of template DNA. Moreover, a no reverse transcriptase control was set up to check for DNA contamination. For positive control, *Leishmania* gDNA was used.

2.3 Preparing and measuring different polymer concentrations

To prepare a 20% Ficoll solution, 10g of Ficoll powder with a molecular weight of 400 kDa (Sigma-Aldrich) was dissolved in 25ml of MilliQ water using low heat and slow magnetic stirring. The solution was then brought to a total volume of 50ml with MilliQ water and subjected to autoclaving for sterilisation. A similar process was repeated with PVP having a molecular weight of 360 kDa (Sigma-Aldrich). Prior to autoclaving, the PVP stock solution underwent dialysis against MilliQ water using dialysis tubing with a 14mm diameter and a 12 kDa cutoff. The dialysis aimed to eliminate small molecular impurities that could be metabolised by cells, potentially enhancing their swimming capacity. The dialysis spanned eight days, with the MilliQ water being changed every other day (Martinez *et al.* (109).

To estimate concentrations, empty eppendorf tubes were initially weighed, and their weights were recorded. Subsequently, these tubes were filled with 1ml of either PVP or Ficoll stock solution, and their weights were recorded again. The filled tubes were then allowed to dry in a VWR INCU-Line® digital incubator at 60°C, and the final weights after drying were recorded. These weights were used to calculate the final concentrations of the polymers as a percentage weight/volume (% w/v).

For maintaining parasite viability, serial dilutions were conducted by mixing an equal volume of polymer with 1X M119 media, following the methodology established in a prior study by Findlay (55). This process was also replicated using Grace's medium.

2.4 Preparing sample chambers

Glass sample chambers were constructed using slides, cover slips, and UV-curing adhesive (Norland 63) (Edmund Optics). The assembled chambers achieved a final sample volume of approximately 26 × 6 × 1.5 mm^3. Curing of the adhesive was carried out under a long- wave UV lamp, rendering the chambers ready to be filled with the requisite parasite cells for holographic microscopy (55).

2.5 fPPG preparation

A volume of 200 - 250 µL of *L. amazonensis* fPPG, with a concentration of 240 µg/µL in PBS (phosphate-buffered saline) obtained from M. E. Rogers at London School of Hygiene and Tropical Medicine, was prepared (59). *L amazonensis*, being genetically close to *L. mexicana* was chosen due to unavailability of *L. mexicana* fPPG for this research. PBS, known for its isotonic and non-toxic properties to cells, was used as the solvent. The stock solution of fPPG underwent serial dilution multiple times in supplemented M199 at a 1:1 ratio, resulting in distinct concentrations for testing, specifically 120 µg/µL, 60 µg/mL, and 30 µg/µL.

2.6 Assay setup

2.6.1 Control data

Fluid volumes of around 100 µL containing either procyclic- or metacyclic-enriched suspensions in M199 medium were introduced into prepared chamber slides. To prevent drift, the slides were sealed with petroleum jelly. Subsequently, the samples were imaged within a 30-minute timeframe.

2.6.2 Motility capture

The sample chambers were loaded with an approximate volume of 300 µL of a solution containing polymer at various concentrations, along with parasite cells diluted to a factor of $5\times10^{4.}$ To prevent drift, the edges of the slides were sealed with vaseline. Imaging of these samples was conducted within a 30-minute timeframe.

2.6.3 fPPG viscosity

With the exception of the reduced sample chamber volume, the fPPG assay mirrored the previously described motility capture assay. Alterations were made to the chamber slides to accommodate an approximate sample volume of 20 µL for each replicate. The final measurements for the modified chamber were approximately $5 \times 6 \times 1.5$ mm³.

2.6.4 Polymer viscosity

A 300 µL solution comprising magnetic beads at varying polymer concentrations was used for the experiment. Video images were captured within a 10-minute period. To ensure homogeneity and prevent settling, the mixture was consistently and thoroughly suspended, with frequent mixing throughout the duration of the experiment.

2.7 Digital inline holographic microscopy video capture

The samples were imaged using a Nikon Eclipse E600 upright microscope, employing a single-mode fibre-coupled laser diode with a peak emission wavelength of 642 nm as the light source. Video recording involved capturing 3000 frames within a 1-minute interval using a Mikrotron MC-1362 monochrome camera, operating at a frame rate of 50 Hz and an exposure period of 100 µs. This exposure duration was carefully chosen to minimise blurring resulting from parasite movement (55). Data acquisition used a 10X bright-field lens with a numerical aperture of 0.3, yielding a field of view measuring 1.44 x 1.44 mm² and a video resolution of 1024 x 1024 pixels². The recorded video images were saved in the form of uncompressed 8-bit AVI files. Each of the three biological replicates comprised four technical samples, aligning with the methodology outlined in the study conducted by Findlay (55). The experimental setup is illustrated in Figure 2.1.

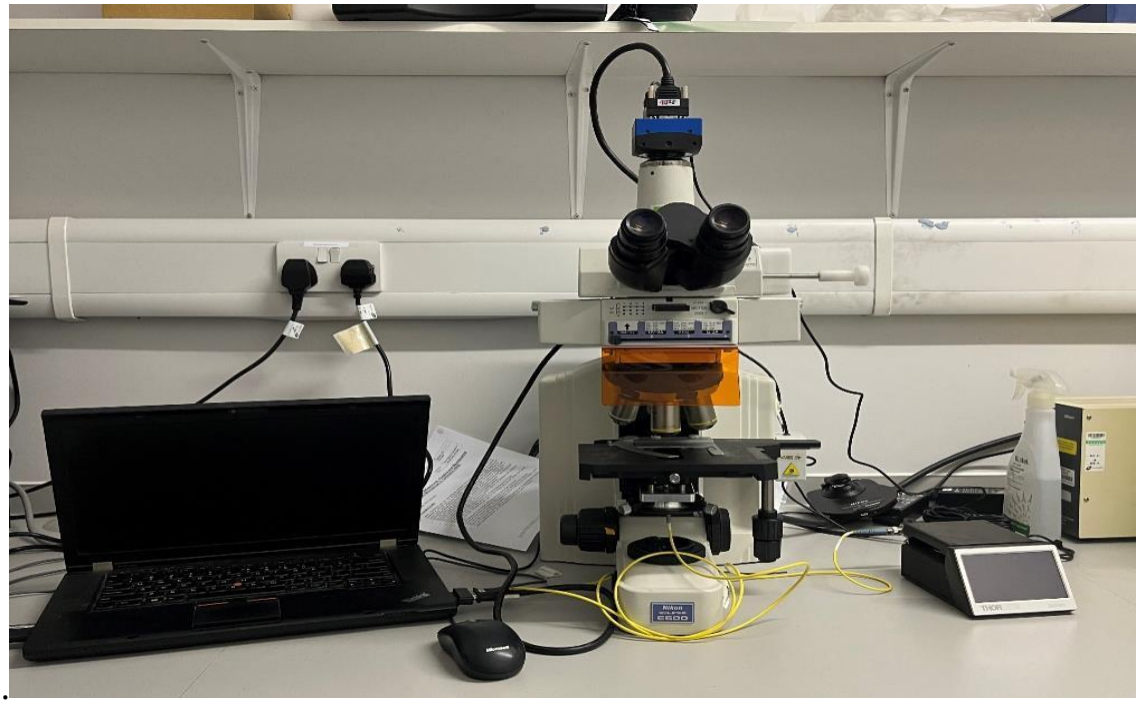

Figure 2.1: Setup for digital inline holographic microscopy

2.8 Determining viscosity of Ficoll, PVP and fPPG using magnetic tweezers

The samples were imaged using a Nikon Eclipse Ti upright microscope, attached to a camera comparable to the one employed in holographic microscopy. Similar frame rates and exposure durations were applied for video recording. The recorded video images were stored in the form of uncompressed 8-bit AVI files. The configuration of the setup is depicted in Figure 2.2.

Figure 2.2: Setup for magnetic tweezers

2.9 Reconstruction

Several steps were involved in the reconstruction of holographic data obtained:

1. Normalisation: This process removed static backdrop features (for example marks on sample chamber surfaces) by dividing each video frame by the background image.

2. Calculating image stack: This mathematically refocused every hologram without a background.

3. 3D image segmentation: For every cell in the frame, this step created a list of (x, y, z) coordinates.

4. Compiling tracks: The position of the parasites in each frame was connected using this procedure to create tracks.

5. Spline smoothing: The data were smoothed in order to provide more accurate measurements of swimming speed (Findlay) (55).

6. Swimmers vs diffusers: Brownian motion, a random diffusive movement with no preferred direction, will be displayed by a huge fraction of the parasites being tracked.

7. Diffusers were removed using a filter so that only the parasites that could swim with propulsion could be investigated.

The steps described above were carried out using in-house programs that have been developed by Wilson lab and are adapted for use in LabVIEW (55).

8. Data analysis: Once the post processing of data is complete, tracks were created. Each track represents the position of a single cell given in x, y and z coordinates since the movement was captured in 3D. The parameters curvature, velocity and helicity were used to describe the observed motility trajectories, with their histograms generated using another program developed in-house by Wilson Lab, making use of splined data.

3 RESULTS

3.1 Relative quantification of *sherp* and *histone h4* relative to *nmt*

Figure 3.1 below illustrates relative quantification for *histone h4* and *sherp* in procyclic promastigote cells and metacyclic promastigote cells, expressed relative to *nmt. Sherp* is upregulated in metacyclic promastigote cells whereas *histone h4* is upregulated in procyclic promastigote cells.

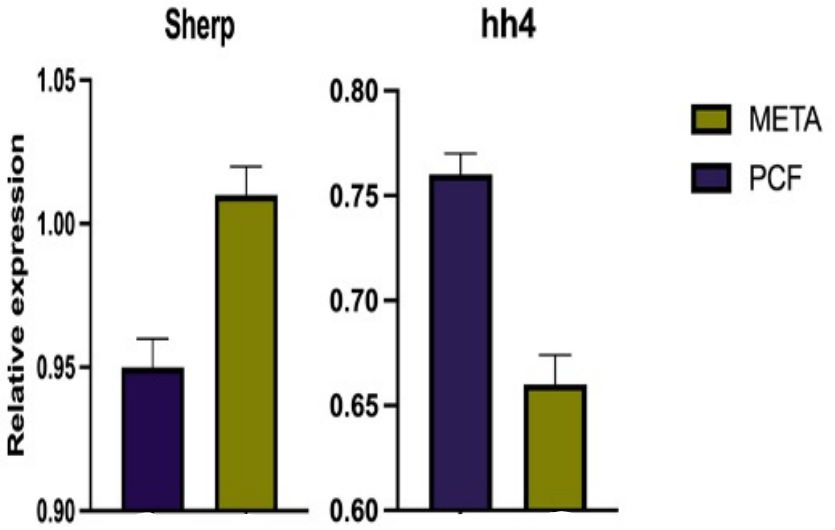

Figure 3.1: Relative expression for sherp and histone h4 (hh4). META represents metacyclic promastigote and PCF procyclic promastigote cells

3.2 Viscosity of Ficoll and PVP in medium

The variation in viscosity across different concentrations of fPPG, Ficoll, and PVP is depicted in Figure 3.2, showing increase in viscosity with rising concentration.

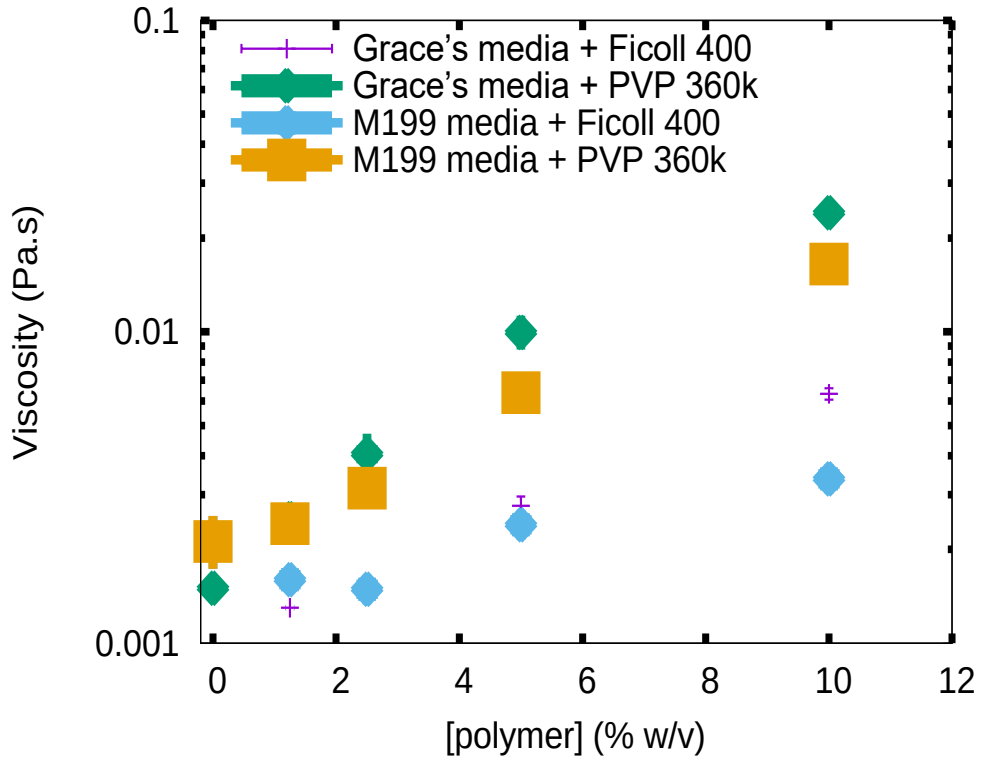

Figure 3.2: Viscosity as a function of polymer concentration (samples prepared by the author and experiments conducted by L.G. Wilson)

3.3 Reconstruction: track data of procyclic promastigote cells in medium

Tracks resulting from the post-processing analysis of procyclic promastigote cells' motility in M119 medium without polymer (control experiment) are depicted in Figure 3.3. This figure represents a compilation of rendered tracks from three different samples, showcasing the helical trajectory from cells that swam the greatest distance. Tracks were created using inhouse programming developed by Wilson lab, which is an established method (55).

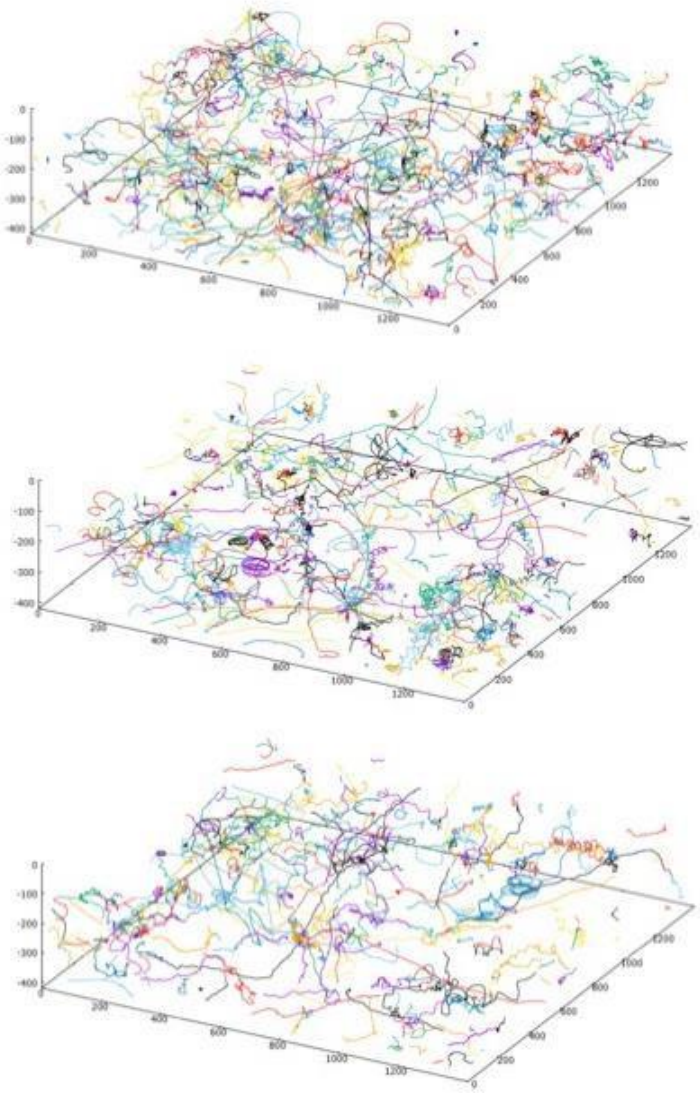

Figure 3.3: Rendered tracks of procyclic promastigote cells, μm$^{3.}$
Three replicates in M119 media without polymer

3.4 Reconstruction: track data of metacyclic promastigote cells in medium.

Figure 3.4 displays tracks resulting from the post-processing analysis of metacyclic promastigote cells' motility in M119 medium without polymer (control experiment). These tracks represent a visualisation of the straight trajectory of rendered tracks from three different samples of cells that swam the greatest distance.

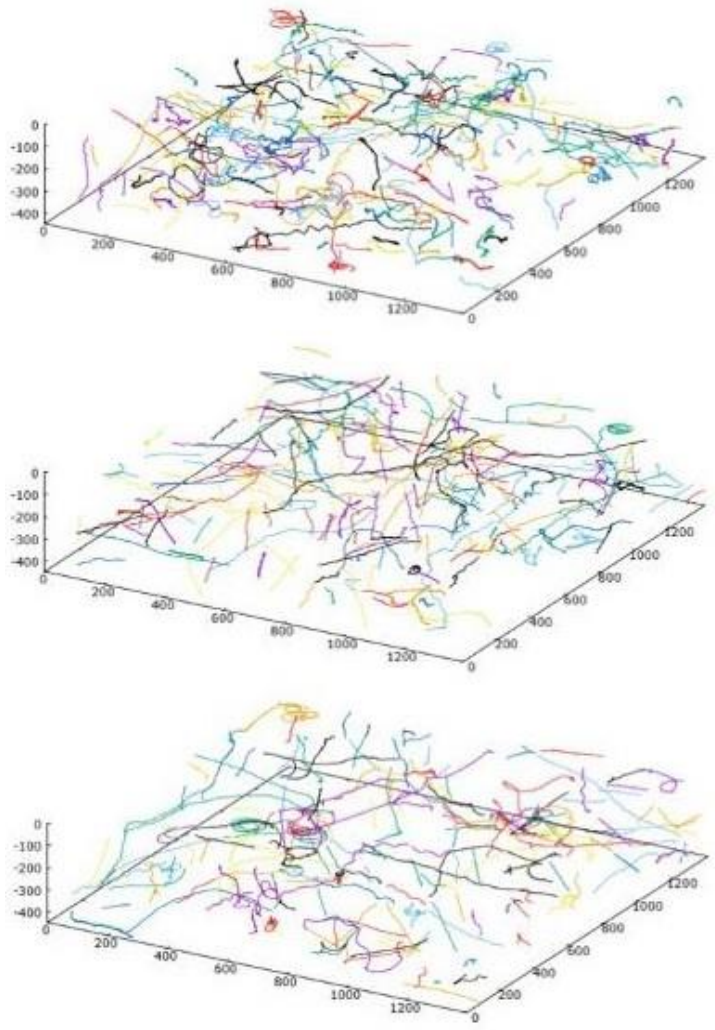

Figure 3.4: Rendered tracks of metacyclic promastigote cells, μm^3
Three replicates in M119 media without polymer

3.5 Speed histograms for procyclic and metacyclic promastigote cells

Histograms were generated through post-processing analysis for procyclic and metacyclic promastigote cells. Speed histograms for procyclic and metacyclic promastigote cells in M119 medium without polymer are depicted in Figures 3.5a and 3.5b. These histograms demonstrate a faster swimming speed in metacyclic promastigote cells compared to procyclic promastigote cells at similar concentration. Statistical analysis using paired T test showed this difference to be significant (The mean swimming speed for metacyclic and procyclic promastigote cells was 17.3 and 11.9 respectively. 95%CI [3.0154,7.8896]).

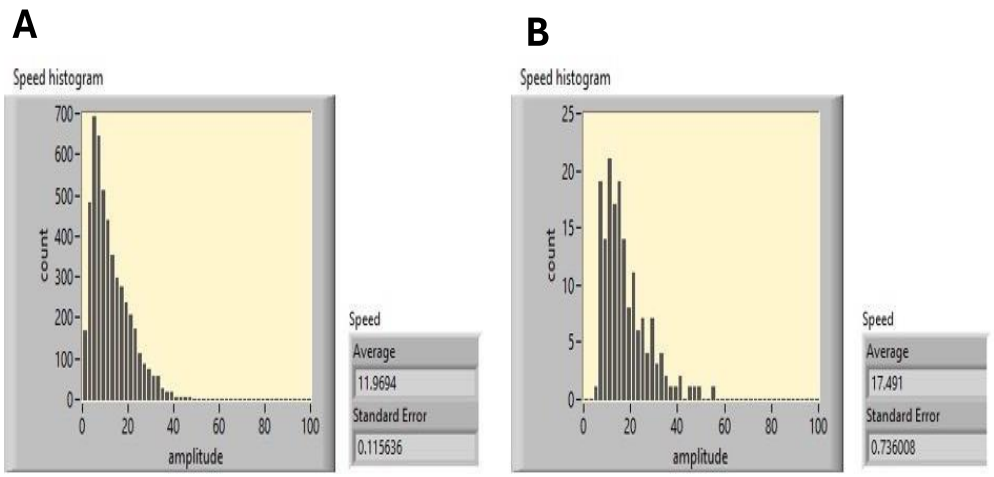

Figure 3.5: Velocity histogram for (A) procyclic and (B) metacyclic promastigote cells

3.6 Curvature histograms for procyclic and metacyclic promastigote cells

Figures 3.6a and 3.6b display curvature histograms for procyclic and metacyclic promastigote cells in M119 medium without polymer. These figures highlight a higher curvature in procyclic promastigote cells compared to metacyclic promastigote cells at similar concentration. Curvature can intuitively show how much the direction of a curve changes over a small distance, thus influencing their overall movement pattern.

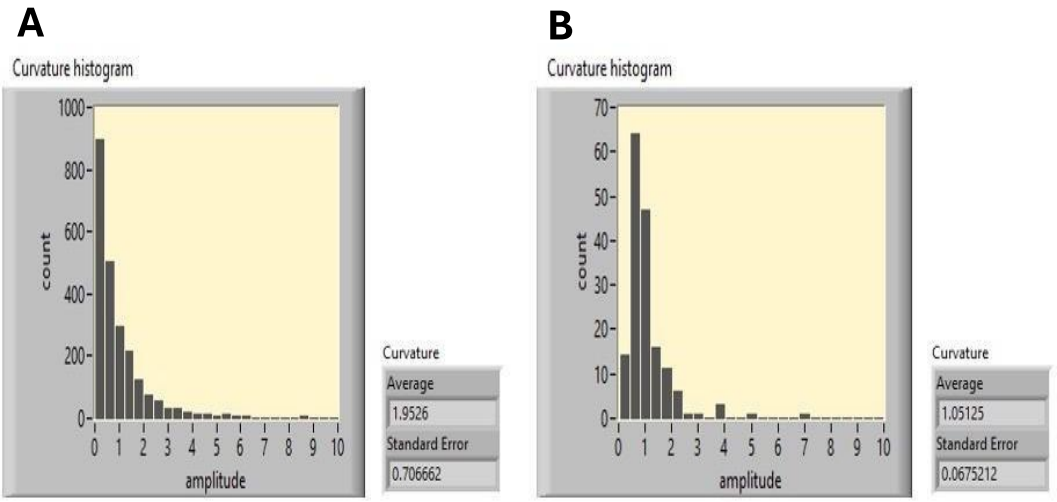

Figure 3.6: Curvature histogram for (A) procyclic and (B) metacyclic promastigote cells

3.7 Helicity histograms for procyclic and metacyclic promastigote cells

Figures 3.7a and 3.7b below represent helicity histograms for procyclic and metacyclic promastigote cells in M119 medium without polymer respectively, demonstrating a symmetrical distribution for both parasite cell populations.

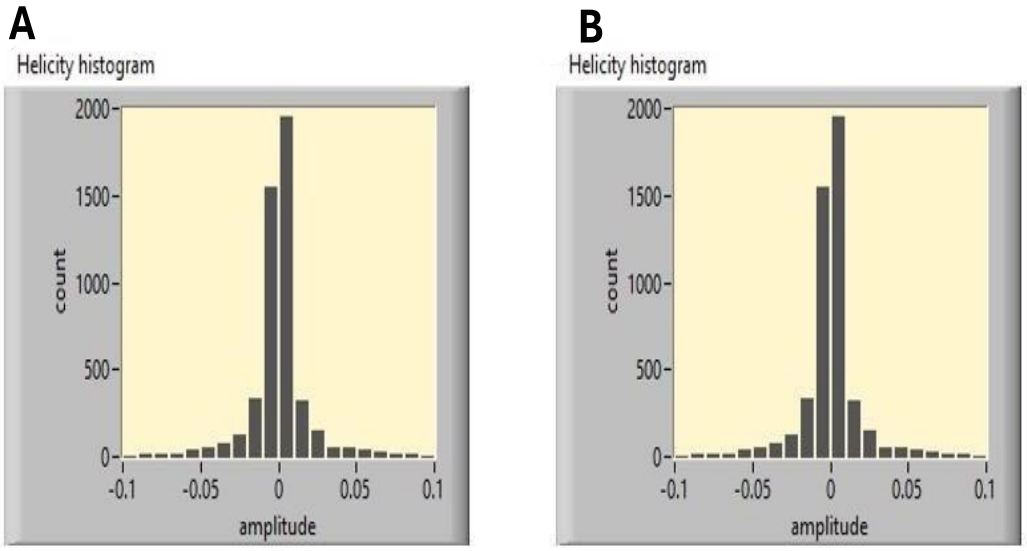

Figure 3.7: Helicity histogram for (A) procyclic and (B) metacyclic promastigote cells

3.8 Average swimming speeds of procyclic and metacyclic promastigote cells in different polymer concentrations

In figure 3.8a, the average swimming speeds of both procyclic and metacyclic promastigote cells are illustrated across various concentrations of Ficoll and PVP. The graph indicates an overall faster swimming speed in metacyclic promastigote cells compared to procyclic promastigote cells. Figures 3.8b and 3.8c provide a detailed comparison, showing the average swimming speeds of metacyclic and procyclic promastigote cells separately within Ficoll and PVP polymers, revealing significantly faster speeds in Ficoll compared to PVP. Polymer concentrations are expressed in %w/v.

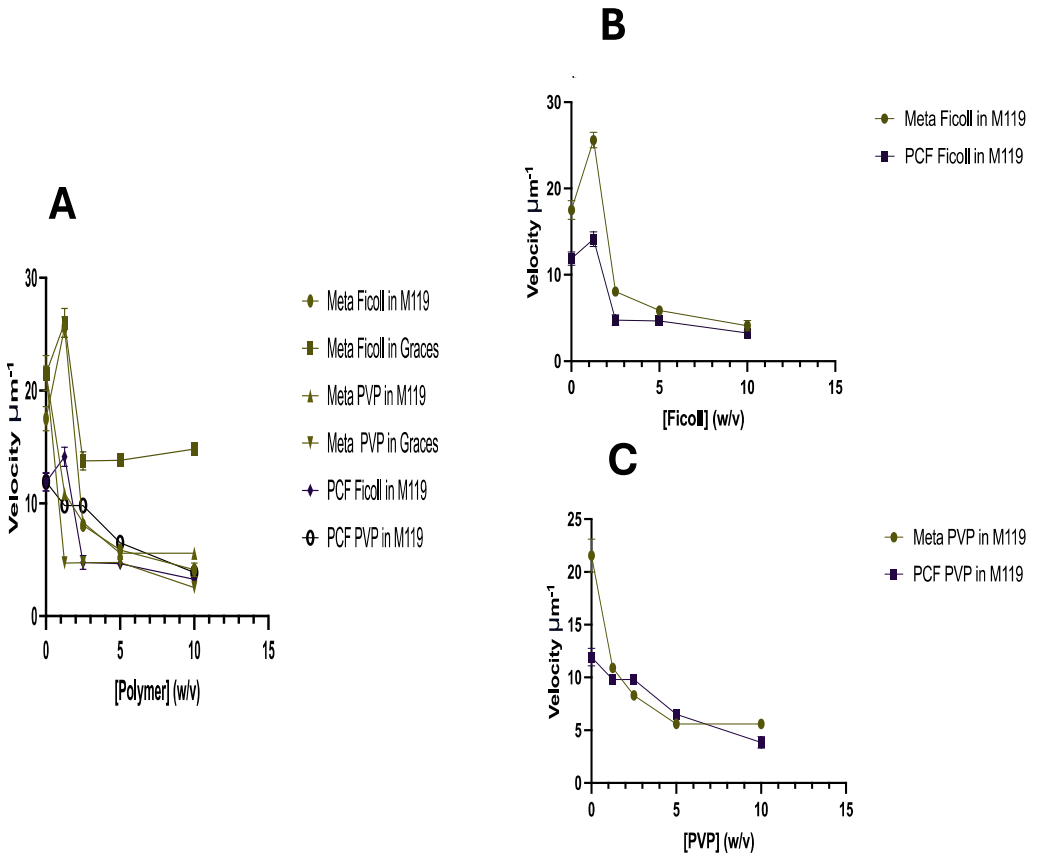

Figure 3.8 (A) Average swimming speeds of parasite cells in different concentrations of Ficoll and PVP (B) In Ficoll (C) In PVP

3.9 Average swimming speeds of parasite cells in different fPPG concentrations

Figure 3.9 depicts the average swimming speeds of metacyclic and procyclic promastigote cells at various concentrations of fPPG, highlighting a decrease in swimming speed with increasing concentration for both parasite cell populations. Two different concentrations of fPPG were used: 120 µg/µL and 30 µg/µL.

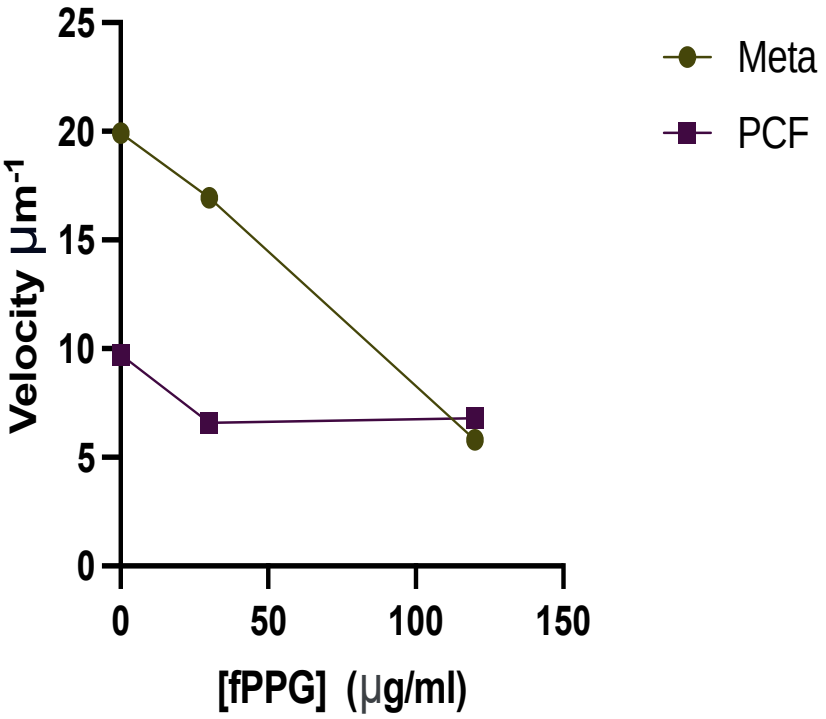

Figure 3.9: Average swimming speeds of parasite cells in different concentrations of fPPG

4 DISCUSSION

Understanding the mechanisms employed by *L. mexicana* to promote motility is crucial due to its significance in the cyclical progression and host transitions, ultimately contributing to disease development (138,139). While closely related trypanosomes, particularly *T. brucei,* have been extensively studied in terms of motility, studies on *Leishmania* motility have not received comparable attention. Recent advancements in the field of parasite motility have sparked renewed interest in the mechanisms of transmission. This research study seeks to contribute to the existing knowledge by investigating the swimming behaviour of *L. mexicana* parasites in solutions with different polymer concentrations. This exploration may have important biomedical implications, shedding light on how this pathogen invades the mucosal lining of mammalian hosts.

4.1 Use of RT-qPCR to validate life cycle stages

In the validation of life cycle stages for *L. mexicana,* three methods—microscopic observation, growth curves, and molecular validation—are applicable, with molecular validation of procyclic and metacyclic promastigote stages using RT-qPCR, being a key objective in this study. *Histone h4* and *sherp* were chosen as molecular markers in this study due to their well-documented and reliable specificity for different life cycle stages in *Leishmania* (55,136). The use of these markers enhances the accuracy and reliability of molecular validation for the respective life cycle stages in *L. mexicana*. *Sherp* is expressed predominantly in metacyclic parasites. It localises to the endoplasmic reticulum and mitochondrion, making it a valuable marker for distinguishing metacyclic promastigotes (140). *Histone h4* expression, in contrast, was discovered to be upregulated in *L. major* procyclic promastigotes (136), leading to its use as a marker for distinguishing procyclic promastigotes in this study.

Figure 3.1 depicts a higher level of *histone h4* gene expression in the procyclic promastigote cells compared to the metacyclic promastigote cells. This is indicative of the procyclic promastigote cells being predominantly in the log-phase, as they have not yet differentiated into later life cycle stages. Conversely, a higher level of *sherp* expression is observed in the metacyclic promastigote cells compared to the procyclic promastigote cells, reflecting the differentiation of parasite cells into this later life cycle stage. These findings align with previous studies (128) and show that the parasites are in the expected life cycle stages.

For the analysis of relative quantification, I used *nmt* as reference. Its expression remains constant in both procyclic and metacyclic promastigote cells, making it a suitable choice for this purpose. This gene has been previously employed in similar studies for its stable expression (128).

For the initiation of qPCR, only a small quantity of target nucleic acid from genomic DNA (gDNA) or cDNA) is necessary. To prevent contamination with reaction inhibitors, I kept the initial template amount to the minimum required for reliable quantification, which was 20µl in this study. Since the starting material was RNA, DNase treatment was employed to eliminate any contaminating DNA from the preparation. UV-Vis (photometry) was used for quantification before and after DNAse treatment. This method is straightforward, requiring no additional sample preparation or dyes, and it offers immediate measurements of purity ratios such as A260/280 and A260/230 (141).

Including appropriate controls in a qPCR experiment is crucial to assess the possibility of false negatives or positives. In my qPCR experiment, I incorporated a minus reverse transcriptase control and water negative controls to test for contaminated DNA, such as genomic DNA or PCR product from a previous run.

Upon analysis of the negative controls, the results were generally as expected. However, fluorescence was detected in the water sample control, indicating the potential presence of contaminants. On the positive control side, a sample of *L. mexicana* genomic DNA was used, and the analysis revealed the expected fluorescence, affirming the reliability of the experiment's positive control. These controls collectively contribute to the validation and interpretation of the qPCR results.

4.2 Relative viscosity of model polymers and fPPG is comparable

The study by Findlay (55) employed rheometry, a traditional method for determining the viscosity of polymers. This approach faced challenges related to the large number of sand flies and the significant amount of dissection time required to obtain the necessary volumes of fPPG. The viscometer used in that study required a sample volume of 16ml for accuracy, making it unsuitable for determining the viscosity of fPPG. To address these challenges, I utilised cutting-edge microrheology approaches in my study, which differ from traditional methods by offering simplicity and versatility. These approaches, moreover, require small sample amounts, making them suitable for situations with limited available material, as was the case with fPPG. MT have emerged as a powerful microrheology platform and have been extensively used in previous studies analysing bacteria motility in polymers (108). To determine the viscosity of Ficoll, PVP and fPPG in different concentrations, MT were used. The absolute viscosity values observed in Ficoll, PVP and fPPG were similar (Figure 3.2), aligning with the visual observation when shaking the tubes—they did not show drastic differences. The concentrations of fPPG were much lower by weight. This consistency supports the notion that fPPG exhibits a filamentous structure. In contrast, Ficoll and PVP molecules are characterised as small, dense globules and large, tenuous structures, respectively. The results suggest that despite the lower mass of fPPG in a sample, the long, stretched-out chains of fPPG form a network throughout the fluid, contributing to an increase in viscosity.

This finding emphasises the unique rheological behaviour of fPPG compared to the model polymers, showcasing the impact of its filamentous structure on the overall viscosity of the fluid.

4.3 Metacyclic promastigotes swim faster than procyclic promastigotes

Although caution must be used when comparing the behaviour of bacteria and eukaryote cells (for example *Leishmania*) given their vastly different mechanisms for achieving motility, representatives of both bacteria and eukaryotic cells are found in similar or even the same physical and hydrodynamic environments (55). Some bacteria have been observed to swim at a faster speed at a particular viscosity. For example, the swimming speed of *Pseudomonas aeruginosa* (a bacterium with a single polar flagellum) increases with viscosity up to a certain point and thereafter decreases. This has also been shown to occur in various other bacterial species (142). The structure of the polymer solutions is thought to cause this behaviour. Bacteria motility is said to be less affected by linear polymers as compared to branched polymers with the same apparent viscosity (143). These cells are capable of pushing polymer chains out of the way and travel more than in pure liquids or branched polysaccharides. Moreover, this also implies that bacteria swimming has evolved to be especially efficient for a particular viscosity.

The velocity of procyclic promastigotes has been analysed in previous studies using different methods. Gadelha *et al* (144), in their study of long term cultured *L. major* promastigote cells using phase contrast video microscopy found the velocity to be around 36 μms−1. In another study on *L. donovani* promastigote cells, Reddy (145) found their mean velocity to be around 26 μms−1, which was significantly lower than that reported by Gadelha *et al.* (144). The difference could be attributed to use of different species and media in the studies. Before the study by Findlay (51), the velocity of metacyclic promastigote cells had not been reported. The study found that the average speed of *L. mexicana* metacyclic promastigotes was 31 μms−1 and that for *L. mexicana* procyclic promastigotes was considerably slower at 19 μms−1.

To reduce variation in this research study, the experimental design was optimised to include at least three biological and four technical replicates for each experimental condition. The average swimming speed for metacyclic promastigotes was determined to be 26μms−1 and that of procyclic promastigotes was 14μms−1. Although the overall speeds are slower, they are consistent with those of Findlay (55), indicating that metacyclic promastigotes swim faster than procyclic promastigotes. Moreover, there were no significant differences in the shape of the speed histograms as the polymer concentration increased. The observed differences in the velocity of these two distinct parasite life cycle stages could be explained using hydrodynamic drag force. The procyclic promastigote cell body has width of approximately 5 to7 μm, which is 2 to 3 times wider than of the metacyclic cell body, which also happens to be more streamlined. This narrower body of metacyclic promastigote cells results in significantly less hydrodynamic drag, allowing them to move more rapidly as seen in Figure 3.8a, 3.8b and 3.8c. Because metacyclic promastigote cells need to be transmitted into the mammalian host for infection, this rapid speed may have biological significance. We can thus conclude that metacyclic promastigotes use a more rapid motile action as compared to procyclic promastigotes.

4.3.1 Polymer concentration affects velocity

The most obvious finding to emerge from the analysis of velocity is that it is affected by polymer concentration. Within Ficoll, as the concentration of polymer and thus the viscosity was increased, the procyclic promastigote speed slowed. However, an anomaly was observed in the average swimming speed of procyclic promastigote cells in 1.4% w/v Ficoll; they swam faster than in M199 media without polymer. A similar trend was observed in metacyclic promasatigote cells. At higher concentrations, there was a decline in average swimming speed for both procyclic and metacyclic promastigote cells (Figure 3.8b). This finding broadly supports the work of Findlay (55) who described a similar trend, suggesting that these cells are more capable of swimming in polymer concentration as compared to medium alone. However, speed decreases with increasing polymer concentration.

It is encouraging to compare these results with those previously reported in bacteria (136) and the more closely related *T. brucei*, (110). These cells were shown to swim faster in viscoelastic environment. However, the ability of the cells to swim faster is somewhat unexpected for viscous solution of Ficoll. This higher average speed in procyclic and metacyclic promastigote cells in 1.4% w/v Ficoll could be a result of the cells being more efficient in swimming in environments of slightly higher viscosity compared to M199 media without polymer (55), suggesting that *Leishmania* promastigote cells may be optimised for swimming in certain viscosity.

Within PVP, as concentration of polymer was increased, the procyclic promastigote cells' swimming speed was decreased as compared to M119 medium without polymer. The same pattern was observed for metacyclic promastigote cells (Figure 3.8c). Both procyclic promastigote and metacyclic promastigote cells are still capable of maintaining some motility in PVP even though it has a higher viscosity than Ficoll.

4.4 Metacyclic promastigotes have a lower curvature compared to procyclic promastigotes

The curvature analysis findings in this study were consistent with those in the study by Findlay (55), indicating that metacyclic promastigote cells exhibit lower curvature compared to procyclic promastigote cells, as shown in Figure 3.6a and 3.6b. This observation held true across different polymer concentrations and aligns with the visual representation in Figures 3.3 and 3.4, where metacyclic promastigote cell tracks appear predominantly as straight lines (Figure 3.4), while procyclic promastigote cell tracks exhibit a helical pattern (Figure 3.3). Notably, the curvature histograms for both procyclic and metacyclic promastigote cells did not show significant changes as polymer concentration increased.

4.5 Metacyclic promastigotes and procyclic promastigotes have symmetrical helicity distribution

The helicity histograms for both procyclic and metacyclic promastigote cells across different polymer concentrations displayed a generally symmetrical distribution with no significant bias toward right or left handedness, as illustrated in Figures 3.7a and 3.7b. This pattern is consistent with findings from a previous study by Findlay (51). Interestingly, the helicity distribution of procyclic promastigote cells was observed to be wider compared to that of metacyclic promastigote cells. One plausible explanation for this observation could be the presence of a "tumble" in the swimming behaviour of metacyclic promastigote cells, as depicted in Figure 3.4.

It's worth noting that, although the 3D nature of the tracks would allow for the calculation of torsion, this parameter was not determined in this study. This is because it can be difficult to interpret and determine its biological relevance.

4.6 Metacyclic promastigotes swim faster in Grace’s medium than in M119 medium

The results regarding the motility of metacyclic promastigote cells in different concentrations of PVP and Ficoll polymers in both M119 and Grace's medium suggest that these cells exhibit greater swimming capability in Ficoll polymer with Grace’s medium compared to the same polymer in M119 medium at comparable concentrations. Faster speeds were observed in Grace’s medium, as depicted in Figure 3.8a. However, this trend was reversed in PVP, where cells demonstrated slower speeds at comparable concentrations. It might be worth speculating that the ionicities of the media are different, which might explain the different swimming behaviours: the polymers change conformation when the local ion concentration is different (i.e. in different media) and either shrink or grow, leading to different viscosity (as seen in Figure 3.2).

4.7 Effect of fPPG concentration on motility of procyclic and metacyclic promastigote cells

The final experiment in this section generated 3D tracks of both procyclic and metacyclic parasites swimming in two different concentrations of fPPG, providing a more biologically significant approach compared to the polymer solution studies. This experiment has the potential to enhance our understanding of how motility influences transmission from female phlebotomine sandflies to mammals.

The average swimming speed analysis revealed that the velocity of both procyclic and metacyclic promastigote cells decreased with increasing fPPG concentration, as shown in Figure 3.9. This finding is somewhat unexpected, especially for procyclic promastigote cells, which would not typically come into contact with PSG within the sand fly's mouthparts.

It is important to interpret these data cautiously since *L. amazonensis* fPPG was used in this study due to unavailability of *L. mexicana* fPPG. While these fPPGs are genetically close, they differ in terms of content and expression (145). Additionally, the study considered only one high and one low concentration of fPPG, and a more diverse range in fPPG concentration could be biologically relevant, particularly for metacyclic promastigote cells.

Upon analysing the curvature and helicity of the tracks, the investigation determined that procyclic and metacyclic promastigote cells display trends similar to those observed in the prior analysis involving polymers. This observation suggests the presence of additional factors influencing motility of the parasite beyond concentration.

5 CONCLUSIONS

5.1 Overall conclusion

In this research study, I have successfully demonstrated distinct swimming behaviours in metacyclic and procyclic promastigote cells of *L. mexicana.* Procyclic promastigote cells exhibit a helical corkscrew-like motion, while metacyclic promastigote cells swim faster and in a straighter pattern, characterised by a run and tumble motion. The faster and more direct motility of metacyclic promastigote cells may be biologically relevant for their transmission, contrasting with the helical motion observed in procyclic promastigote cells. This suggests that the differentiation during metacyclogenesis not only alters the morphology of *Leishmania* parasites but also influences their mode of motility (55).

Interestingly, these distinct swimming patterns appear to be unaffected by changes in polymer concentration and viscosity. While the velocity of *Leishmania* procyclic and metacyclic promastigote cells is influenced by varying viscosity, their curvature and helicity remain relatively consistent. This observation implies that factors beyond physical properties may play a role in influencing parasite motility (perhaps pH and temperature).

MT were used to determine the previously unknown viscosity of fPPG, underscoring its distinct rheological attributes in comparison to model polymers.

Furthermore, my research study has used RT-qPCR to validate lifecycle stages which is an important quality control step for obtaining robust data.

5.2 Suggestions for future work

Holographic microscopy, an advanced high-throughput imaging method, was employed in my research to investigate the impact of viscosity on the motility of *Leishmania.* The findings provide insights that could be extrapolated to other external conditions the parasite encounters during its life cycle, such as variations in temperature, offering valuable information for potential targets in future treatments and therapeutics.

While the main components of fPPG are well understood, many other molecules and proteins within PSG remain unidentified. Future studies in *Leishmania* motility would greatly benefit from additional information on the structure and physical properties of these components for more accurate comparisons (55). Establishing a fPPG-deficient parasite line could significantly enhance testing the importance of PSG in transmission (67). Recent advancements in gene editing tools, such as CRISPR-Cas9, offer promising avenues for research aimed at identifying and validating genes and proteins contributing to *Leishmania* motility and their ability to sense environmental stimuli.

Although DIHM is not yet ready for in vivo studies, the rapid pace of technological advancement suggests that it may not be long before this technique can be applied to track the motility of *Leishmania* promastigotes in their natural hosts in 3D. The prospect of testing whether the swimming patterns observed in this study align with in vivo observations adds an intriguing dimension to future research.

In conclusion, this research project provides an interesting model for motility studies and is important to understand the biology of the parasite for developing new control tools.

6 REFERENCES

1. Gebremichael D, Girma Z & Keskes S. A review on biology, epidemiology and public health significance of leishmaniasis. *J Bacteriol Parasitol* .2013;04:1-

2. [Accessed 2024 May 20]. Available from: https://www.who.int/leishmaniasis.

3. World Health Organization. Investing to overcome the global impact of neglected tropical diseases. World Health Organization. 2015.

4. Rezvan H, Nourian A & Navard S. An Overview on *Leishmania* Diagnosis. *JoMMID*.2017;5(1And 2):1-11.

5. Giuseppe A, Annastella F, Giannetto C, Elisabetta G, Giuseppe P, BarbaraT, CiceroL, Cassata G, & Simona, D. Preliminary study for the application of Raman spectroscopy for the identification of *Leishmania* infected dogs. *Scientific reports*. 2022;*12*(1), 7489.

6. Cardo LJ. *Leishmania*: risk to the blood supply. *Transfusion.* 2006 ;46(9):1641-5.

7. Steverding D. The history of leishmaniasis. *Parasit Vectors.* 2017;10(1).

8. Shaw J. The leishmaniases - survival and expansion in a changing world. A mini- review. *Mem Inst Oswaldo Cruz.* 2007; 102:541–7.

9. King A. In search of a vaccine for leishmaniasis [published online ahead of print, 2023. *Nature*. 2023;10.1038/d41586-023-02580-y.

10. Mondal DK, Pal DS, Abbasi M, Datta R. Functional partnership between carbonic anhydrase and malic enzyme in promoting gluconeogenesis in *Leishmania major*. *FEBS J*. 2021;288(13):4129-4152.

11. Leishmaniasis [Accessed 2023Feb 15] available from http:///www.who.int/mediacentre/factsheets/fs375/en.

12. Bennis I, Thys S, Filali H, De Brouwere V, Sahibi H, Boelaert M. Psychosocial impact of scars due to cutaneous leishmaniasis on high school students in Errachidia province, Morocco. *Infect Dis Poverty*. 2017;6(1).

13. Nagle AS, Khare S, Kumar AB, Supek F, Buchynskyy A, Mathison C. Recent developments in drug discovery for leishmaniasis and human African trypanosomiasis. *Chem Rev*. 2014;114(22):11305–47.

14. David CV, Craft N. Cutaneous and mucocutaneous leishmaniasis (3). *Dermatol Ther*. 2009;22:491–502.

15. Bañuls A, Bastien P, Pomares C, Arevalo J, Fisa R, Hide M. Clinical pleiomorphism in human leishmaniases, with special mention of asymptomatic infection. *Clinical Microbiology and Infection*. 2011;17(10):1451–61.

16. Torres-Guerrero E, Quintanilla-Cedillo MR, Ruiz-Esmenjaud J, Arenas R. Leishmaniasis: a review. *F1000Res*. 2017; 6:750.

17. Palumbo E. Treatment strategies for mucocutaneous leishmaniasis. J *Glob Infect Dis.* 2010;2(2):147–50.

18. Bravo F, Sanchez MR. New and re-emerging cutaneous infectious diseases in Latin America and other geographic areas. *Dermatol Clin*. 2003;21(4):655–68.

19. Maltezou HC. Drug resistance in visceral leishmaniasis. *J Biomed Biotechnol*. 2010; 2010:617521.

20. Pasha F, Saleem S, Nazir T, Tariq J, Qureshi K. Visceral Leishmaniasis (Kala- Azar): A Triumph Against a Trickster Disease. *Cureus*. 2022;14(6).

21. Chappuis F. Visceral leishmaniasis: what are the needs for diagnosis, treatment and control? *Nature Reviews.* 2007; 5:7–10.

22. Pigott DM, Bhatt S, Golding N, Duda KA, Battle KE, Brady OJ, et al. Global distribution maps of the leishmaniases. *Elife.* 2014;3.

23. Zijlstra EE. The immunology of post-kala-azar dermal leishmaniasis (PKDL). *Parasit Vectors*. 2016;9(1).

24. [Accessed 2023 Feb 24] Available from https://www.researchgate.net/publications/34762892.

25. Barrett MP, Croft SL. Management of trypanosomiasis and leishmaniasis. *Br Med Bull.* 2012;104(1):175–96.

26. Petersen CA. Leishmaniasis, an emerging disease found in companion animals in the United States. *Top Companion Anim Med*. 2009;24(4):182-188.

27. Von Stebut E. Leishmaniasis. *JDDG J der Dtsch Dermatologischen Gesellschaft.*2015;13(3):191–201.

28. Sundar S, Rai M. Laboratory diagnosis of visceral leishmaniasis. *Clin Diagn Lab Immunol.* 2002;9(5):951–8.

29. Maxfield L, Crane JS. Leishmaniasis. [Updated 2023 Jun 28]. In: StatPearls. Treasure Island (FL): StatPearls Publishing; 2023. Jan. Available from: https://www.ncbi.nlm.nih.gov/books/NBK531456/.

30. Chappuis F, Sundar S, Hailu A, Ghalib H, Rijal S, Peeling RW. Visceral leishmaniasis: what are the needs for diagnosis, treatment and control? *Nat Rev Microbiol.* 2007;5(11):873–82.

31. Lockwood D, Sundar S. Serological tests for visceral leishmaniasis. *Br Med J.*2006;333(7571):711–2.

32. Croft SL, Seifert K, Yardley V. Current scenario of drug development for leishmaniasis. *Indian J Med Res.* 2006; 123:399–410.

33. Chakravarty J, Sundar S. Drug resistance in leishmaniasis. *J Glob Infect Dis*. 2010;2(2):167–76.

34. Croft SL, Sundar S, Fairlamb AH. Drug resistance in leishmaniasis. *Clin Microbiol Rev.* 2006;19(1):111–26.

35. Martin Sainz de la Maza, O. Leishmaniasis transmission biology: Role of Promastigote Secretory Gel as a transmission determinat. 2014. https://researchonline.lshtm.ac.uk/id/eprint/1775854/.

36. Bern C, Maguire JH, Alvar J. Complexities of assessing the disease burden attributable to leishmaniasis. *PLOS.* 2008; 2:1–8.

37. Osman M, Mistry A, Keding A, Gabe R, Cook E, Forrester S, et al. A third-generation vaccine for human visceral leishmaniasis and post kala azar dermal leishmaniasis: First-in-human trial of ChAd63-KH. *PLoS Negl Trop Dis.* 2017;11(5).

38. Killick-Kendrick R. The Biology and Control of phlebotomine sand flies. *Clin Dermatol*. 1999; 17:279–89.

39. Chappuis F. Visceral leishmaniasis: what are the needs for diagnosis, treatment, and control? *Nature Reviews.* 2007; 5:7–10.

40. Alexander B, Maroli M. Control of phlebotomine sandflies. *Med Vet Entomol*.2003;17(1):1-18.

41. Nagi N. Bangladesh eliminates visceral leishmaniasis. *Lancet Microbe*. 2024; 5(5): e420.

42. Sacks D, Kamhawi S. Molecular aspects of parasite-vector and vector-host interactions in leishmaniasis. *Annu Rev Microbiol.* 2001; 55:453–83.

43. CDC-Centers for Disease Control, Prevention. CDC - Leishmaniasis - Biology. 2010 Aug 15 [Accessed 2023 Feb https://www.cdc.gov/parasites/leishmaniasis/biology.html.

44. Sunter J, Gull K. Shape, form, function and *Leishmania* pathogenicity: from textbook descriptions to biological understanding. *Open Biol.* 2017;7(9).

45. Serafim TD, Figueiredo AB, Costa PAC, Marques-da-Silva EA, Gonçalves R, de Moura SAL, *et al*. *Leishmania* metacyclogenesis is promoted in the absence of purines. *PLoS Negl Trop Dis.*2012;6(9).

46. Oliveira AS, Aredes-Riguetti LM, Pereira BAS, Alves CR, Souza-Silva F. Degron pathways and leishmaniasis: debating potential roles of *Leishmania* spp. proteases activity on guiding hosts immune response and their relevance to the development of vaccines. *Vaccines (Basel)*. 2023;11(6):1015.

47. Souza D, Souto-Padron W. The paraxial structure of the flagellum of *Trypanosomatidae. The Journal of Parasitology.* 1980;66(2).

48. Antoine JC, Prina E, Jouanne C, Bongrand P. Parasitophorous vacuoles of *Leishmania amazonensis*-infected macrophages maintain an acidic pH. *Infect Immun.* 1990;58(3):779–87.

49. Leishmaniasis [Accessed 2323 Aug 2] Available from https://www.cdc.gov/dpdx/leishmaniasis/index.html.

50. Matthews KR. Controlling and coordinating development in vector-transmitted parasites. *Science.* 2011;331(6021):1149–53.

51. Landfear S, Ignatushchenko M. The flagellum and flagellar pocket of trypanosomastids. *Molecular and Biochemical Parasitology*. 2001;115(1):1-17.

52. Wheeler RJ, Gluenz E, Gull K. Basal body multipotency and axonemal remodelling are two pathways to a 9+0 flagellum. *Nat Commun.* 2015;6(1).

53. Gluenz E, Ginger ML, McKean PG. Flagellum assembly and function during the *Leishmania* life cycle. *Curr Opin Microbiol.* 2010;13(4):473-9.

54. Brokaw CJ. Bending moments in free-swimming flagella. *J Exp Biol*. 1970;53(?2):445-464.

55. Findlay Rachel. Investigating Motility of *Leishmania mexicana*; its impact on. parasite lifecycle progression and infectivity. Rachel Christina Findlay. 2018. https://etheses.whiterose.ac.uk/23681/1/ThesisV4.pdf.

56. Vargas-Parada L. Kinetoplastids and their networks of interlocked DNA. *Nature Education*. 2010;3(9).

57. Yilmaz IC, Dunuroglu E, Ayanoglu IC, Ipekoglu EM, Yildirim M, Girginkardesler N, et al. *Leishmania* kinetoplast DNA contributes to parasite burden in infected macrophages: Critical role of the cGAS-STING-TBK1 signaling pathway in macrophage parasitemia. *Front Immunol.* 2022;13.

58. Figarella K, Uzcategui N, Zhou Y, Lefurgey A, Ouellette M, Bhattacharjee H, et al. Biochemical characterization of *Leishmania major* aquaglyceroporin LmAQP1: possible role in volume regulation and osmotaxis. *Molecular Microbiology.* 2007;65(4):1006–17.

59. Rogers ME, Chance ML, Bates PA. The role of promastigote secretory gel in the origin and transmission of the infective stage of *Leishmania mexicana* by the sandfly *Lutzomyia longipalpis*. *Parasitology.* 2002; 124:495–507.

60. Field M, Carrington M. The trypanosome flagellar pocket. *Nature Reviews Microbiology.* 2009;7(11):775–86.

61. Bates PA. Transmission of *Leishmania* metacyclic promastigotes by phle botomine sand flies. *International Journal for Parasitology.* 2007;37(10):1097–106.

62. Maroli M, Feliciangeli M, Bichaud L, Charrel R, Gradoni L. Phlebotomine sandflies and the spreading of leishmaniases and other diseases of public health concern. *Medical and Veterinary Entomology.* 2012;27(2):123–47.

63. Ready PD. Biology of phlebotomine sand flies as vectors of disease agents. *Annu Rev Entomol.* 2013; 58:227–50.

64. Kwakye-Nuako G, Mosore M, Duplessis C, Bates M, Puplampu N, Mensah- Attipoe I, *et al.* First isolation of a new species of *Leishmania* responsible for human cutaneous leishmaniasis in Ghana and classification in the *Leishmania enriettii* complex. *International Journal for Parasitology*. 2015;45(11):679–84.

65. Dougall A, Alexander B, Holt D, Harris T, Sultan A, Bates P, et al. Evidence incriminating midges (Diptera: Ceratopogonidae) as potential vectors of *Leishmania* in Australia. *International Journal for Parasitology.* 2011;41(5):571–9.

66. Schlein Y, Jacobson R. Sugar meals and longevity of the sandfly *Phlebotomus papatasi* in an arid focus of *Leishmania major* in the Jordan Valley. *Medical and Veterinary Entomology.* 1999;13(1):65–71.

67. Telleria E, Araújo A, Secundino N, Avila-Levy C, Traub-Csekö Y. Trypsin-Like Serine Proteases in *Lutzomyia longipalpis* - Expression, Activity and Possible Modulation by *Leishmania infantum chagasi. PLoS ONE.* 2010;5(5).

68. Dillon R, Ivens A, Churcher C, Holroyd N, Quail M, Rogers M, et al. Analysis of ESTs from *Lutzomyia longipalpis* sand flies and their contribution toward understanding the insect-parasite relationship. *Genomics.* 2006;88(6):831–40.

69. Tang Y, Ward R. Sugar feeding and fluid destination control in the phlebotomine sandfly *Lutzomyia longipalpis* (Diptera: Psychodidae). *Medical and Veterinary Entomology.* 1998;12(1):13–9.

70. Stoffolano J, Haselton A. The Adult dipteran crop: A unique and overlooked organ. *Annual Review of Entomology*. 2013;58(1):205–25.

71. Rogers ME. The role of *Leishmania* proteophosphoglycans in sand fly transmission and infection of the mammalian host. *Frontiers in Microbiology.* 2012; 3:1–13.

72. Abdeladhim M, Kamhawi S, Valenzuela JG. What's behind a sand fly bite? The profound effect of sand fly saliva on host hemostasis, inflammation and immunity. *Infect Genet Evol.* 2014 Dec; 28:691–703.

73. Kamhawi S. Phlebotomine sand flies and *Leishmania* parsites:friends or foe? *Trends Parasitrol.* 2006; 22:439-45.

74. Rogers ME. *Leishmania* chitinase facilitates colonization of sand fly vectors and enhances transmission to mice. *Cell Microbiol*. 2008; 10:1363–72.

75. Sundar S. Failure of pentavalent antimony in visceral leishmaniasis in India: report from the centre of the Indian epidemic. *Clin Infect Dis.* 2000; 31:1104-7.

76. Secundino N. Proteophosphoglycan confers resistance of Leishmania major to midgut digestive enzymes induced by blood feeding in vector sand flies. *Cell Microbiol.* 2010; 12:906–18.

77. Doehl JSP, Sádlová J, Aslan H, Pružinová K, Metangmo S, Votýpka J, *et al. Leishmania* HASP and SHERP genes are required for in vivo differentiation, parasite transmission and virulence attenuation in the host. *PLoS Pathog*. 2017 ;13(1).

78. Walters LL, Modi GB, Chaplin GL, Tesh RB. Ultrastructural development of Leishmania chagasi in its vector, *Lutzomyia longipalpis* (Diptera: Psychodidae). *Am J Trop Med Hyg.* 1989;41:295–317.

79. Dost´alov´a A and Volf P. *Leishmania* development in sand flies: Parasite-vector interactions overview. *Parasites and Vectors*.2O12;5(1).

80. Rogers ME, Llg T, Nikolaev AV, Ferguson MAJ, Bates PA. Transmission of cutaneous leishmaniasis by sand flies is enhanced by regurgitation of fPPG. *Nature.* 2004; 430:463–7.

81. Carmichael S, Powell B, Hoare T, Walrad PB, Pitchford JW. Variable bites and dynamic populations; new insights in *Leishmania* transmission. *PLoS Negl Trop Dis.* 2021;15(1).

82. Serafim TD, Coutinho-Abreu IV, Oliveira F, Meneses C, Kamhawi S, Valenzuela JG. Sequential blood meals promote *Leishmania* replication and reverse metacyclogenesis augmenting vector infectivity. *Nature Microbiology*. 2018;1–8.

83. Bates PA. Revisiting *Leishmania*'s life cycle. *Nat Microbiol.* 2018;3(5):539-30.

84. Beverley SM, Turco SJ. Lipophosphoglycan (LPG) and the identification of virulence genes in the protozoan parasite *Leishmania*. *Trends Microbiol.* 1998;6(1):35

85. McConville MJ, Mullin KA, Ilgoutz SC, Teasdale RD. Secretory pathway of trypanosomatid parasites. *Microbiol Mol Biol Rev*. 2002;66(1):122–54.

86. De Assis RR, Ibraim IC, Nogueira PM, Soares RP, Turco SJ. Glycoconjugates in New World species of *Leishmania* polymorphisms in lipophosphoglycan and glycoinositolphospholipids and interaction with hosts. *Biochim Biophys Acta.* 2012;1820(9):1354–65.

87. Sacks DL. The role of phosphoglycans in *Leishmania*- sand fly interactions. *Proc Natl Sci USA.* 2000; 97:406-11.

88. Svobodova P, Dvorakova M. Bloodmeal digestion and Leishmania major infections in *Phlebotomus duboscqi:* effect of carbohydrates inhibiting midgut lectin activity. *Med Vet Entomol.* 2001; 15:281–6.

89. Puentes SM, Silva RP, Sacks DL, Hammer CH, Joiner KA. Serum resistance of metacyclic stage *Leishmania major* promastigotes is due to release of C5b-9. *Journal of immunology*. 1990;145(12):4311–6.

90. Wilson R. Stage-specific adhesion of *Leishmania* promastigotes to sand fly midguts assessed using an improved comparative binding assay. *PLoS Negl Trop Dis*. 2010;4(9).

91. Killick-Kendrick R, Molyneux DH, Ashford RW. *Leishmania* in phlebotomid sandflies. I. Modifications of the flagellum associated with attachment to the mid- gut and oesophageal valve of the sandfly. *Proc R Soc Lond B Biol Sci.* 1974; 187:409–19.

92. Sacks DL, Silva D. The generation of infective stage Leishmania major promastigotes is associated with the cell-surface expression and release of developmentally regulated glycolipid. *J Immunol*. 1987; 1:3099–106.

93. Rogers ME, Bates PA. *Leishmania* manipulation of sand Fly feeding behaviour results in enhanced transmission. *PLoS Pathog.* 2007;3.

94. Stierhof YD. Filamentous proteophosphoglycan secreted by *Leishmania* promastigotes forms gel-like three-dimensional networks that obstruct the digestive tract of infected sandfly vectors. *Eur J Cell Biol.* 1999; 78:675–89.

95. Rogers ME, Chance ML, Bates PA. The role of promastigote secretory gel in the origin and transmission of the infective stage of *Leishmania mexicana* by the sand fly *Lutzomyia longipalpis. Parasitology*. 2002; 124:495–507.

96. Gossage SM, Rogers ME, Bates PA. Two separate growth phases during the development of *Leishmania* in sand flies: implications for understanding the life cycle. *Int J Parasitol.* 2003;33(10):1027–34.

97. Gir E. *Leishmania* proteophosphoglycans regurgitated from infected sand flies accelerate dermal wound repair and ex- acerbate leishmaniasis via insulin-like growth factor 1-dependent signalling. *PLoS Pathogens*. 2018;14(1).

98. Shortt HE, Swaminath CS. The method of feeding of *Phlebotomus argentipes* with relation to its bearing on the transmission of Kala-Azar. *Indian J Med Res.* 1927; 15:827.

99. Serafim, T. D., Coutinho-Abreu, I. V., Dey, R., Kissinger, R., Valenzuela, J. G., Oliveira, F., & Kamhawi, S. (2021). Leishmaniasis: the act of transmission. *Trends in parasitology*, *37*(11), 976–987.

100. Bates PA. *Leishmania* sand fly interaction: progress and challenges. *Curr Opin Microbiol.* 2008; 11:340–4.

101. Rogers M. Proteophosophoglycans regurgitated by *Leishmania*-infected sand flies target the L-arginine metabolism of host macrophages to promote parasite survival. *PLoS Pathog*. 2009;5.

102. Kamhawi S. The biological and immunomodulatory properties of sand fly saliva and its role in the establishment of *Leishmania* infections. *Microbes Infect.* 2000; 2:1765–73.

103. Valenzuela JG, Belkaid Y, Garfield MK, Mendez S, Kamhawi S, Rowton ED, et al. Toward a defined anti-*Leishmania* vaccine targeting vector antigens. *J Exp Med.* 2001;194(3):331–42.

104. Bray D. Cell movements: from molecules to motility. New York: Garland Science; 2001.

105. Beneke T, Demay F, Hoo E, Lestinova T, Shafiq J, Sadlova P, *et al. Leishmania* flagellar proteome demonstrates requirement for directional motility in sandfly infections. PLOS Pathogens. 2019;15(6).

106. Lawyer PG. Development of Leishmania major in Phlebotomous duboscoi and Sergentomyia achwetzi(Diotera: Psychodidae). Am J Trop Hyg. 1990; 43:31-43.

107. Saraiva EM. Changes in lipophosphoglycan and gene expression associated with the development of *Leishmania major* in *Phlebotomus papatasi. Parasitology*. 1995; 111:275–87.

108. Helmenstine AM. What Is a Polymer? [Internet]. [Accessed 2023 Aug 3]. Available from: https://www.thoughtco.com/definition-of-polymer-605912.

109. Martinez VA, Schwarz-Linek J, Reufer M, Wilson LG, Morozov AN, Poon WCK. Flagellated bacterial motility in polymer solutions. Proceedings of the National Academy of Sciences. 2014;111(50):17771–6.

110. [Internet]. [Accessed 2023 Aug 2] Available from: https://www.sigmaaldrich.com/GB/en/technical documents/protocol/cell-culture-and-cell-culture-analysis/primary-cell-culture/ficoll-400.

111. Nair B. Final report on the safety assessment of polyvinylpyrrolidone (PVP). *Int J Toxicol.* 1998 ;17(4_suppl):95–130.

112. Sankaranarayanan K, Meenakshisundaram N. Micro-viscosity induced conformational transitions in poly-L-lysine. *Royal Society of Chemistry Advances.* 2016;6(78):74009–17.

113. Zhang D, Li X, Tan H, Zhang G, Zhao Z, Shi H, et al. Photocatalytic reduction of Cr(VI) by polyoxometalates/TiO2 electrospun nanofiber composites. *Royal Society of Chemistry Advances.* 2014;4(84):44322–6.

114. Heddergott N, Krüger T, Babu SB, Wei A, Stellamanns E. Trypanosome motion represents an adaptation to the crowded environment of the vertebrate bloodstream. *PLOS Pathogens.* 8(11).

115. Uppaluri S, Nagler J, Stellamanns E, Heddergott N, Herminghaus S, Engstler M, et al. Impact of microscopic motility on the swimming behavior of parasites: straighter trypanosomes are more directional. *PLoS Computational Biology*. 2011;7(6):1–8.

116. Weiße S, Heddergott N, Heydt M, Pflästerer D, Maier T, Haraszti T, *et al.* A quantitative 3D motility analysis of *Trypanosoma brucei* by use of digital in-line holographic microscopy. *PLoS One.* 2012;7(5): e37296.

117. Molaei M, Barry M, Stocker R, Sheng J. Failed escape: solid surfaces prevent tumbling of *Escherichia coli. Phys Rev Lett.* 2014 ;113(6) :068103.

118. Jikeli JF, Alvarez L, Friedrich BM, Wilson LG, Pascal R, Colin R, Pichlo M, Rennhack A, Brenker C, Kaupp UB. Sperm navigation along helical paths in 3D chemoattractant landscapes. *Nat Commun*. 2015; 6:7985.

119. Schnars WU. Direct recording of holograms by a CCD target and numerical reconstruction. *Applied optics.* 1994;33(2):179–81.

120. Thornton KL, Findlay RC, Walrad PB, Wilson LG. Investigating the swimming of microbial pathogens using digital holography. *Adv Exp Med Biol*. 2016; 915:17-32.

121. Cheong FC, Wong CC, Gao Y, *et al*. Rapid, high-throughput tracking of bacterial motility in 3D via phase-contrast holographic video microscopy. *Biophys J*. 2015;108(5):1248-1256.

122. Lee S-H, Grier DG. Holographic microscopy of holographically trapped three- dimensional structures. *Optics express.* 2007;15(4):1505–12.

123. Kim MK. Principles and techniques of digital holographic microscopy. *J Photonics Energy.* 2010 Apr 1;018005

124. Wilson LG, Zhang R. 3D Localization of weak scatterers in digital holographic microscopy using Rayleigh-Sommerfeld back-propagation. O*ptics Express.* 2012;20(15).

125. Instantaneous speed and instantaneous velocity [Internet]. BYJUS. BYJU'S; 2019 [Accessed 2023 Feb 23]. Available from:https://byjus.com/physics/instantaneous-speed-and-instantaneous-velocity/.

126. Frenet serret formulas. [Accessed 2023 Feb 23]. Available from: https://en.wikipedia.org/wiki/Frenet–Serret_formulas.

127. Difference between chirality and helicity [Internet]. Compare the Difference Between Similar Terms. Differencebetween.com; 2020 [Accessed 2023 Feb 23]. Available from: https://www.differencebetween.com/difference-between-chirality- and-helicity/.

128. Findlay RC, Osman M, Spence KA, Kaye PM, Walrad PB, Wilson LG. High- speed, three-dimensional imaging reveals chemotactic behaviour specific to human- infective *Leishmania* parasites. *Elife.* 2021 Jun 28;10.

129. Wilson LG, Poon WCK. Small-world rheology: an introduction to probe-based active microrheology. *Phys Chem Chem Phys*. 2011;13(22):10617–30.

130. Gaire S, Fabian R Jr, Pegg I, Sarkar A. Magnetic tweezers: development and use in single-molecule research. *Biotechniques*. 2022;72(2):65-72.

131. Hosu BG, Jakab K, Bánki P, Tóth FI, Forgacs G. Magnetic tweezers for intracellular applications. *Rev Sci Instrum.* 2003 Sep;74(9):4158–63.

132. Sarkar R, Rybenkov VV. A guide to magnetic tweezers and their applications. *Front Phys.* 2016 6;4.

133. .Bustin S. A-Z of Quantitative PCR. IUL Biotechnology Series. 2004.

134. Basic principles of RT-qPCR [Accessed 2023 Aug 7] Available from https://www.thermofisher.com/uk/en/home/thermoscientific/molecular biology/molecular-biology-learning-centre/molecular-biology-resource library/spotlight-articles/basic-principles-rt-qpcr.html.

135. RT-qPCR [Accessed 2023 Aug 7]. Available from https://www.sigmaldrich.com/GB/en/technical-documents/technical articles/genomics/qpcr/quantitative-pcr-and-digitalpcr-detection-methods.

136. de Pablos LM, Ferreira TR, Dowle AA, Forrester S, Parry E, Newling K, et al. The mRNA-bound proteome of *Leishmania mexicana:* Novel genetic insight into an ancient parasite. *Mol Cell Proteomics.* 2019 Jul;18(7):1271–84.

137. Späth GF, Beverley SM. A lipophosphoglycan-independent method for isolation of infective *Leishmania* metacyclic promastigotes by density gradient centrifugation. *Exp Parasitol*. 2001;99(2):97-103.

138. Rogers M, Kropf P, Choi B-S, Dillon R, Podinovskaia M, Bates P, et al. Proteophosophoglycans regurgitated by *Leishmania*-infected sand flies target the L- arginine metabolism of host macrophages to promote parasite survival. P*LoS Pathog.* 2009 ;5(8):

139. Rogers ME, Corware K, Müller I, Bates PA. Leishmania infantum proteophosphoglycans regurgitated by the bite of its natural sand fly vector, *Lutzomyia longipalpis,* promote parasite establishment in mouse skin and skin-distant tissues. *Microbes Infect.* 2010;12(11):875–9.

140. Knuepfer E, Stierhof Y-D, Mckean PG, Smith DF, Kean P. Characterization of a differentially expressed protein that shows an unusual localization to intracellular membranes in *Leishmania major*. *Biochem J*. 2001; 356:335–44.

141. RNA/DNA quantification - UK. [Accessed 2023 Aug 24]; Available from:https://www.thermofisher.com/uk/en/home/life-science/dna-rna-purification-analysis/nucleic-acid-quantitation.html.

142. Schneider WR, Doetsch RN. Effect of Viscosity on Bacterial Motility. *Journal of Bacteriology*. 1974;71(8):3253–4.

143. .Berg HC, Turner L. Movement of microorganisms in viscous environments. *Nature*. 1979;278(5702):349–51.

144. Gadelha C, Wickstead B, Gull K. Flagellar and ciliary beating in trypanosome motility. *Cell Motility and the Cytoskeleton.* 2007;64(8):629–43.

145. Reddy GS, Mukhopadhyay AG, Dey CS. The p38 MAP kinase inhibitor, PD 169316, inhibits flagellar motility in *Leishmania donovani. Biochemical and Biophysical Research Communications.* 2017;493(4):1425–9.